The Meteoritical Society

Meteoritics & Planetary Science 1–25 (2013)
doi: 10.1111/maps.12109

Isotopic and chemical variation of organic nanoglobules in primitive meteorites

Bradley T. De GREGORIO[1,2*], Rhonda M. STROUD[2], Larry R. NITTLER[3], Conel M. O'D. ALEXANDER[3], Nabil D. BASSIM[2], George D. CODY[4], A. L. David KILCOYNE[5], Scott A. SANDFORD[6], Stefanie N. MILAM[7], Michel NUEVO[6,8], and Thomas J. ZEGA[9]

[1]Nova Research, Inc., Alexandria, Virginia 22308, USA
[2]Materials Science and Technology Division, Naval Research Laboratory, Washington, District of Columbia 20375, USA
[3]Department of Terrestrial Magnetism, Carnegie Institution of Washington, Washington, District of Columbia 20015, USA
[4]Geophysical Laboratory, Carnegie Institution of Washington, Washington, District of Columbia 20015, USA
[5]Advanced Light Source, Lawrence Berkeley National Laboratory, Berkeley, California 94720, USA
[6]NASA Ames Research Center, Moffett Field, California 94035, USA
[7]Astrochemistry Laboratory, NASA Goddard Space Flight Center, Greenbelt, Maryland 20771, USA
[8]SETI Institute, Mountain View, California 94043, USA
[9]Lunar and Planetary Laboratory, Department of Planetary Sciences, University of Arizona, Tucson, Arizona 85721, USA
[*]Corresponding author. E-mail: bradley.degregorio.ctr@nrl.navy.mil

(Received 02 May 2012; revision accepted 19 February 2013)

Abstract–Organic nanoglobules are microscopic spherical carbon-rich objects present in chondritic meteorites and other astromaterials. We performed a survey of the morphology, organic functional chemistry, and isotopic composition of 184 nanoglobules in insoluble organic matter (IOM) residues from seven primitive carbonaceous chondrites. Hollow and solid nanoglobules occur in each IOM residue, as well as globules with unusual shapes and structures. Most nanoglobules have an organic functional chemistry similar to, but slightly more carboxyl-rich than, the surrounding IOM, while a subset of nanoglobules have a distinct, highly aromatic functionality. The range of nanoglobule N isotopic compositions was similar to that of nonglobular ^{15}N-rich hotspots in each IOM residue, but nanoglobules account for only about one third of the total ^{15}N-rich hotspots in each sample. Furthermore, many nanoglobules in each residue contained no ^{15}N enrichment above that of bulk IOM. No morphological indicators were found to robustly distinguish the highly aromatic nanoglobules from those that have a more IOM-like functional chemistry, or to distinguish ^{15}N-rich nanoglobules from those that are isotopically normal. The relative abundance of aromatic nanoglobules was lower, and nanoglobule diameters were greater, in more altered meteorites, suggesting the creation/modification of IOM-like nanoglobules during parent-body processing. However, ^{15}N-rich nanoglobules, including many with highly aromatic functional chemistry, likely reflect preaccretionary isotopic fractionation in cold molecular cloud or protostellar environments. These data indicate that no single formation mechanism can explain all of the observed characteristics of nanoglobules, and their properties are likely a result of multiple processes occurring in a variety of environments.

INTRODUCTION

Hollow, spherical, micrometer-sized carbonaceous features were first observed in powdered samples of the Orgueil and Ivuna carbonaceous chondrite meteorites (Claus and Nagy 1961; Rossignol-Strick and Barghoorn 1971; Alpern and Benkheiri 1973), although an extraterrestrial origin for these features could not be satisfactorily established due to the possibility of extensive terrestrial biological contamination (Tasch 1963). Nearly 40 years later, carbonaceous "nanoglobules" were independently reported in the Tagish Lake meteorite and several other carbonaceous chondrites (Nakamura et al. 2002; Garvie and Buseck 2004), including Orgueil (Garvie 2006), and are now routinely observed in studies of chondritic organic

© The Meteoritical Society, 2013.

matter (e.g., Floss and Stadermann 2009; Floss et al. 2011; Herd et al. 2011). Nanoglobules in Tagish Lake were shown to contain isotopic enrichments in both D and ^{15}N (Nakamura-Messenger et al. 2006). Subsequently, carbonaceous nanoglobules have been reported in other primitive astromaterials, such as interplanetary dust particles (IDPs; Messenger et al. 2008; Busemann et al. 2009; Matrajt et al. 2012), Antarctic micrometeorites (Maurette 1998; Aoki and Akai 2008) and cometary dust collected by the NASA Stardust mission (Brownlee et al. 2006; Matrajt et al. 2008, 2010; De Gregorio et al. 2010).

Nanoglobules are primarily composed of organic C, with minor amounts of O, N, and S (Garvie and Buseck 2004; Garvie 2006). Although the abundances of these minor light elements vary for different nanoglobules in a given meteorite by up to approximately 10 atom%, the average nanoglobule composition is similar to that of bulk organic matter in the meteorite (Garvie and Buseck 2004; Garvie 2006). Electron energy-loss spectroscopy (EELS) performed with a transmission electron microscope (TEM) indicates that nanoglobules from many different meteorites are all composed primarily of structurally disordered polycyclic aromatic organic matter (Garvie and Buseck 2004; Garvie 2006). Raman and infrared spectroscopy, on the other hand, suggest that nanoglobules in the Tagish Lake meteorite consist of aliphatic and oxidized organic matter (Nakamura et al. 2002). A preliminary report on synchrotron-based X-ray absorption near-edge structure (XANES) spectroscopy of nanoglobules in the Murchison meteorite indicated that their organic chemistry can vary significantly (De Gregorio et al. 2010). Of the two Murchison nanoglobules described in that study, one was composed of organic matter with similar chemical functional groups to the bulk insoluble organic matter (IOM) in the meteorite, while the other nanoglobule was composed of distinctly more polyaromatic organic matter.

Although many researchers have speculated on their formation mechanisms, the origin of organic nanoglobules is unknown. For example, the large D and ^{15}N isotopic enrichments present in many nanoglobules suggest that the organic matter, or its precursor material, formed through ion-molecule reactions or ice-grain interactions in extremely cold (approximately 10 K) regions of dense interstellar molecular clouds, or the outer regions of the solar nebula (Nakamura-Messenger et al. 2006; De Gregorio et al. 2010; Matrajt et al. 2012). Nakamura-Messenger et al. (2006) proposed that the globular morphology could have arisen through aggregation of isotopically enriched organic matter on spherical ice grains, after which the ice sublimated to leave hollow globular objects. However, a trivial way to produce spherical, organic features is through interaction with liquid water (Dworkin et al. 2001; Cody et al. 2011), which would most likely occur on asteroid parent bodies. Yet such a postaccretionary origin, which would tend to create objects with similar chemistry, cannot easily account for the observed nanoglobule isotopic anomalies or their elemental and isotopic heterogeneity. In addition, a comprehensive study of the Tagish Lake carbonaceous chondrite indicates that the more hydrothermally altered lithologies contain significantly fewer nanoglobules (Herd et al. 2011).

Alternatively, Saito and Kimura (2009) showed that nanoglobule-like objects may form from polycyclic aromatic hydrocarbon (PAH) precursors in plasmas around evolved stars, and such an origin would imply that nanoglobules are a type of presolar, circumstellar grain. Such a high-temperature origin, however, is difficult to reconcile with their relatively enriched D and ^{15}N abundances. Spherical, presolar, C-rich grains have been previously identified in residues from carbonaceous chondrites (Bernatowicz et al. 1996; Croat et al. 2005), but such materials are graphitic in nature, with layered "onion-like" and "cauliflower-like" textures, and they often contain carbide or other refractory subgrains. Presolar graphite grains are thus clearly distinct from the organic-rich, homogenous, single-shell structure of a typical nanoglobule.

Previous studies of nanoglobules have been mostly limited to a single meteorite sample or planetary object, in which the particular alteration history of the parent body may have a pronounced effect, or surveyed a limited number of nanoglobules in a few meteorite samples. In this study, we attempted to investigate as large a population of nanoglobules as possible across several chondrite classes and alteration histories to reveal broad characteristics regarding the prevalence, chemistry, and origin of these poorly understood features. We have characterized the morphology, functional chemistry, and isotopic composition of organic nanoglobules from seven primitive meteorites by correlated TEM, scanning-transmission X-ray microscopy (STXM), and secondary ion mass spectroscopy (SIMS). Early results on nanoglobules in the Murchison CM2 carbonaceous chondrite were described previously in De Gregorio et al. (2010).

SAMPLES AND METHODS

Organic nanoglobules were identified and analyzed in existing IOM residues isolated from chips of the host meteorites by iterative dissolution in HCl and CsF (Alexander et al. 2007). Recent in situ studies of carbonaceous chondrites (e.g., Peeters et al. 2012) have

Table 1. Number of nanoglobules analyzed in this study and by each analytical technique.

Meteorite	Type	Total	TEM	STXM	SIMS
Orgueil	CI1	7	7	4	5
Murchison	CM2	17	17	16	6
Bells	CM2	34	24	11	25
Grosvenor Mountains (GRO) 95577	CR1	19	16	10	12
Elephant Moraine (EET) 92042	CR2	24	22	8	9
Queen Elizabeth Range (QUE) 99177	CR2	57	57	16	4
Allan Hills (ALH) 77307	CO3.0	26	26	10	3
TOTAL		184	169	75	64

indicated that this acid dissolution procedure does not significantly change the chemistry of the IOM, although important details regarding spatial relationships between mineral grains and IOM are lost. The seven meteorite residues were chosen for this study (Table 1) to focus on the most primitive carbonaceous chondrite classes, either because they represent the bulk composition of the solar nebula (e.g., Orgueil) or because their bulk IOM has large isotopic excesses in D and/or ^{15}N (Alexander et al. 2007). Because of previously demonstrated connections between localized D and ^{15}N enrichments ("hotspots") and nanoglobule locations (Nakamura-Messenger et al. 2006; Messenger et al. 2008), residues having large isotopic excesses were selected to test the hypothesis that they would contain the largest concentration of organic nanoglobules. In addition, IOM residues were chosen to span the range of aqueous parent-body alteration (types 1, 2, and 3) to reveal any effect on nanoglobule chemistry and/or morphology that might be associated with hydrothermal processing.

Fresh TEM/STXM sections were prepared from IOM residues by ultramicrotomy. Each IOM residue powder was added to a molten S droplet heated to approximately 110 °C, after which the heat source was turned off to allow the droplet to cool and solidify around the sample, usually within a minute. It is unlikely that brief exposure to this temperature causes any structural or chemical changes to the meteoritic IOM, which has already experienced parent-body heating to similar temperatures (Cody et al. 2008). Similarly, comparisons of S-embedded samples with those prepared by alternative methods (e.g., Bassim et al. 2012) have not revealed the generation of new S-bearing organic bonds. The crystallized S droplet was then attached to an epoxy stub with a small amount of cyanoacrylate adhesive. Samples were sectioned in an ultramicrotome with a diamond knife to a thickness of 90–100 nm to ensure both electron transparency (for TEM) and observable transmission of "soft" X-rays (for STXM). Ultramicrotome sections were placed on 200-mesh, Cu, "slim-bar," TEM grids with a thin SiO support film. The S was later sublimated from the sections by gently heating at 60 °C overnight.

Transmission Electron Microscopy

Organic nanoglobules were initially identified in ultramicrotomed IOM sections with a 200 keV JEOL 2200FS field-emission TEM at the Naval Research Laboratory (NRL). Samples were observed in conventional "bright field" mode under low-dose conditions to reduce the potential for chemical alteration of the sample induced by electron irradiation. This was accomplished by using small condenser apertures, low magnifications, and reducing exposure time to the electron beam. The residues were only observed in "low mag" mode (magnifications of 50× through 1500×), except when images of individual nanoglobules were required, at which time the lowest magnification of "high mag" mode was used (4000×). Since electron fluence to the sample was measured to be about an order of magnitude larger at 4000× magnification than in "low mag" mode, exposure of nanoglobules to the electron beam at this magnification was limited by (1) acquiring an image as soon as the nanoglobule was centered on the camera sensor, (2) setting the image acquisition time to 1 second, and (3) closing the gun valve immediately after completing the image acquisition. The gun valve was not reopened to allow electrons to transmit through the sample until the nanoglobule was moved out of the path of the beam. In most cases, nanoglobules were only exposed to the 4000× electron beam for a few seconds or less, which exposed the samples to a total electron fluence of approximately 10^3 electrons nm^{-2} at a flux of about 2 mA cm^{-2}. Subsequent XANES comparison of IOM exposed at this total fluence and unexposed IOM indicated that operating at these minimal electron dose conditions does not induce any detectable changes in the organic functional chemistry of the sample.

The total numbers of nanoglobules identified by TEM in each IOM residue are listed in Table 1, but these data cannot be used to estimate the actual abundance of nanoglobules in each meteorite due to sampling bias and uncertainty in the area normalization. Nanoglobules were identified primarily for other, lower resolution analyses (STXM and SIMS), and therefore the largest nanoglobules, partially isolated from the surrounding IOM and located near the edge of IOM sections (providing the necessary background spectra for XANES), were preferred. This selection

criterion caused a sampling bias against nanoglobules in the interior of the ultramicrotome sections and those whose outer diameters were smaller than the average diameter for each sample. In addition, to minimize the radiation exposure of the sample, only images of areas containing the selected globules were recorded, rather than the total area observed to locate the globules. Thus, the value of the total area needed to normalize the abundance data is unknown.

Scanning-Transmission X-ray Microscopy

Once mapping of nanoglobule locations with TEM was completed, the IOM residues were analyzed by synchrotron-based STXM instruments at either beamline 5.3.2 at the Advanced Light Source, Lawrence Berkeley National Laboratory, USA (Kilcoyne et al. 2003), or beamline 10ID-1 at the Canadian Light Source, University of Saskatchewan, Canada (Kaznatcheev et al. 2007). Each of these instruments utilizes Fresnel zone plate optics to focus an X-ray source down to about a 30 nm spot. Raster images generated with this size beam are inadequate to robustly resolve nanoglobules from other semispherical features in IOM. Therefore, the initial TEM mapping described above was required to identify authentic nanoglobules in the samples.

Nanoglobule C-XANES spectra were acquired by varying the incoming X-ray photons between 270 eV and 340 eV and recording the absorption of photons by the sample at each position coordinate. Spectra were acquired in one-dimensional "linescan" mode or, more often, in 2-D "image stack" mode, where the average X-ray absorption was averaged over a selected region of pixels in a series of aligned images (Jacobsen et al. 2000). The energy shift between subsequent X-ray images could be variably controlled by a spherical grating monochromator and was selected to be 0.1 eV in the region of the C 1*s* absorption edge between 284 eV and 292 eV, where the diagnostic $1s \rightarrow 2p\ \pi^*$ spectral features are located. Because the incident "soft" X-ray photons have relatively low energies around the C photo-ionization edge, significant C bond breakage or formation was not expected, although irradiation damage has been shown to occur in some beam-sensitive organic matter during STXM analyses (Cody et al. 2009; Wirick et al. 2009; Nuevo et al. 2011). In our samples, no X-ray damage effects or amorphous C deposition were observed except after long dwell time scans, which prompted a reduction in dwell time for future scans. Even in these cases, the damage/deposition must have been minimal, as no unusual or unaccountable spectral features were observed in the XANES data from these long-dwell-time scans. In addition, no characteristic spectral features were observed due to the cyanoacrylate adhesive used in sample preparation. XANES data analysis, including subtraction of the background photo-absorption from the SiO support film, was performed using the custom software suite aXis2000 (A. Hitchcock et al., http://unicorn.mcmaster.ca/aXis2000.html).

Secondary Ion Mass Spectrometry

Carbon and N isotopic compositions of the nanoglobules were measured after TEM and STXM analysis with a Cameca NanoSIMS 50L ion microprobe at the Department of Terrestrial Magnetism, Carnegie Institution of Washington. The same TEM grids used for XANES analysis were attached to Al stubs with colloidal Ag paint and then coated with a thin (<100 nm) film of Au to eliminate charging effects. Some grids were also back-coated with Au in an attempt to strengthen the substrate, postponing the inevitable failure of the support film under primary ion bombardment. IOM areas containing previously identified nanoglobules were analyzed by rastering a 1 pA primary ion beam of 16 kV Cs^+ ions over 25–100 μm^2 areas with simultaneous collection of secondary ions and secondary electrons in multicollection imaging mode. For most of the measurements, $^{12}C^-$, $^{13}C^-$, $^{12}C^{14}N^-$, $^{12}C^{15}N^-$, and $^{28}Si^-$ were collected. For IOM from ALH 77307 and QUE 99177, $^{12}C^-$, $^{16}O^-$, $^{12}C^{12}C^-$, $^{12}C^{13}C^-$, $^{12}C^{14}N^-$, $^{12}C^{15}N^-$, and $^{28}Si^-$ were collected and C isotope ratios were determined from the C_2 signals. The use of C_2 rather than C ions allows better alignment of the C and N isotopic secondary beams in the mass spectrometer, due to the differing energy distributions of single ions and molecular ions, and in many cases increases the statistical precision of the measurements. Typically, 128 × 128 pixel images were collected with a dwell time of 5 ms/pixel; multiple (10–150) image frames were collected for each area and co-added following image alignment. Before image acquisition, samples were presputtered with a higher intensity Cs^+ beam (tens of pA) to locally remove the Au coating and increase secondary ion yields. The presputtering time was interactively set for each image by manually observing when secondary ion signals reached constant values.

The effective spatial resolution of the NanoSIMS images was about 150 nm, set both by the beam size and uncertainty in the alignment of image frames. At this resolution, only the largest nanoglobules were clearly visible in SIMS secondary electron or ^{12}C ion images, and therefore careful alignment of SIMS and TEM images (with Adobe Photoshop) was essential for defining nanoglobule regions. Unfortunately, warping of the TEM grid support films in some cases made such

alignment impossible, and thus isotopic data are not available for all the nanoglobules that were measured. Isotopic compositions for image subregions, which typically included one or more nanoglobules and other nearby isotopic hotspots, were determined with the L'image software package (L. Nittler, Carnegie Institution of Washington). The samples were, for the most part, completely consumed by the C and N measurements, precluding further NanoSIMS analyses (e.g., D/H ratios).

Although meteoritic IOM is isotopically heterogeneous in H and N on a submicron scale, these variations average out on a scale of several microns (Busemann et al. 2006), allowing a bulk isotopic composition to be measured. Thus, the instrumental fractionation of N isotopic ratios was calibrated by measuring 10–20 μm fragments of IOM from some of the same residues pressed into Au foils and comparing the average measured isotopic ratios to the well-established bulk isotopic compositions (Alexander et al. 2007). The initial measurement of a pressed fragment of ^{15}N-enriched IOM generally gave a significantly lower (by 10–30%) average ^{15}N/^{14}N ratio than the true ratio, but repeated measurements and/or additional presputtering resulted in measured ratios that were consistent with the known bulk values (within 10–20‰ instrumental mass fractionation). This most likely reflects some level of surface adsorption of terrestrial N on the porous IOM samples that requires significant sputtering to remove. This problem was observed to be more severe for several of the ultramicrotomed IOM samples, consistent with their higher surface/volume ratio. Specifically, the average measured δ^{15}N values for sections of four residues (Bells, EET 92042, GRO 95577, and QUE 99177) were systematically lower than the known bulk values. Figure 1 illustrates this problem—each point represents the average and standard deviation of several areas of IOM. Both the magnitude of the discrepancy and the constant ratio of the measured δ^{15}N value to the known value are too large to be explained by a change in instrumental fractionation between samples on TEM grids and particles pressed into Au foils. Nor is the discrepancy correlated to the age of the residues. Rather, as for the pressed particles, the most likely explanation is that it reflects surface-adsorbed terrestrial N contamination. Due to the extremely high surface area of the microtomed IOM, combined with the approximately 100 nm thickness of the samples and the fragile support film, it is not possible to sputter the TEM samples long enough to fully remove this contamination before either the material is gone or the substrate fails. Thus, a consistent correction method is necessary for the SIMS measurements to obtain more accurate δ^{15}N values.

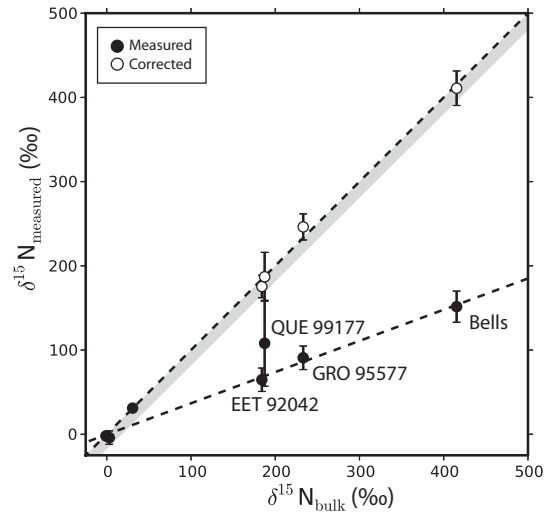

Fig. 1. Comparison of measured δ^{15}N values in bulk IOM with previously reported values (Alexander et al. 2007). Data points represent the average and standard deviation of several 5 × 5 μm regions of IOM from each meteorite. For four IOM residues (EET 92042, GRO 95577, Bells, and QUE 99177), the measured values are significantly lower than the actual value, outside the possible range of instrumental mass fractionation (gray region). These data are consistent with a large component of the measured signal originating as isotopically normal N, most likely adsorbed terrestrial N_2. Data for three of the bulk measurements (EET 92042, GRO 95577, and Bells) that lie on the same line were corrected based on the assumption that 64% of the measured N is contamination. The value for QUE 99177 was corrected assuming a contamination contribution of 39%.

The constant ratios of the measured δ^{15}N values to the true ones for samples measured during the same analytical session (Fig. 1) indicates a relatively constant amount of N contamination in the measurements. We corrected the measured ratios for these samples by multiplying the measured delta values by factors of 2.71 (Bells, EET 92042, and GRO 95577) and 1.64 (QUE 99177) such that the resulting average isotope ratios were consistent with the previously measured bulk values. However, it is unknown whether the N contamination is uniformly present across the IOM samples and thus whether the same correction factors should be applied equally to the individual nanoglobule measurements, which may have different adsorption rates for terrestrial contamination. Therefore, both corrected and uncorrected N isotope data are provided. The true isotopic compositions of the nanoglobules in these four IOM residues are likely somewhere in between these values. Note that it is only possible to infer the presence of such contamination in samples with known nonterrestrial bulk N isotopic conditions. Similar problems may affect the IOM residues whose bulk ^{15}N/^{14}N ratios are close to the terrestrial ones (e.g., Murchison and ALH 77307), but in such cases

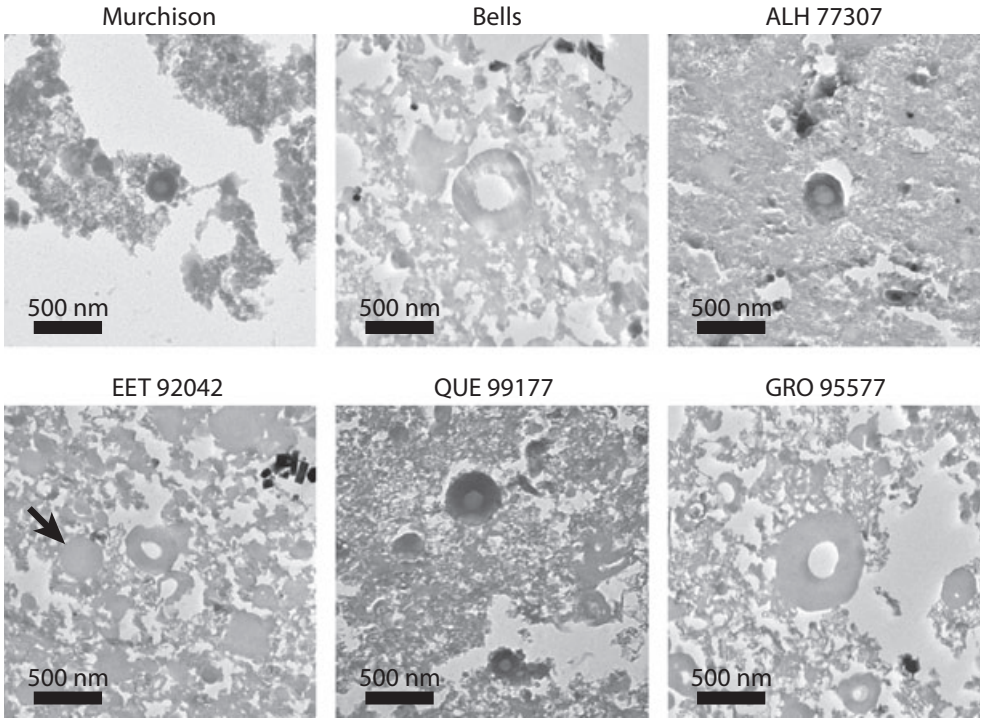

Fig. 2. TEM images of "standard" hollow nanoglobules in six IOM residues. All images were acquired at the same magnification. The nanoglobule shown from Bells contains roughly parallel fractures, indicating a more brittle material. A solid nanoglobule (arrow) is adjacent to the central nanoglobule shown from EET 92042.

one cannot distinguish between contamination and instrumental mass fractionation. Most previous NanoSIMS measurements of N isotopes in TEM samples of meteoritic materials were corrected with terrestrial standards (e.g., Nakamura-Messenger et al. 2006; Matrajt et al. 2008, 2012). It is possible that some of these measurements are also affected by an unknown amount of terrestrial N contamination and thus previously reported ^{15}N enrichments in porous, high surface area samples should be viewed as lower limits.

The instrumental mass fractionation of C isotopic ratios was calibrated based on both epoxy and IOM standards. A C coating was inadvertently applied to the sample side of the Murchison IOM TEM grid, and thus C isotopic data are not available for this sample.

RESULTS

Nanoglobule Morphology

In low-magnification, bright-field TEM images, the dense, homogenous material composing carbonaceous nanoglobules can easily be distinguished from the porous texture of the surrounding IOM. All IOM residues in this study contain nanoglobules with a typical spherical shape and a central void (Fig. 2). The residues also contain abundant solid nanoglobules, which do not contain a central void, and the occasional compound globule, often an aspherical mass with multiple spherical voids. No contact boundaries were observed within the compound globules, indicating that they either formed with multiple hollow interiors, or that a small nanoglobule cluster has fully coalesced into a single globular object. These morphologies are consistent with those described previously (Garvie and Buseck 2004; Garvie et al. 2008). In addition, many nanoglobules were observed to have unusual morphological characteristics, including vermiform or tubular features; extremely thick or thin walls; double walls (e.g., a hollow globule surrounding a solid globule); and thin, rind-like coatings that have partially separated from the globule (Fig. 3). Tubular morphologies were previously reported in Tagish Lake IOM (Garvie and Buseck 2004). IOM from the CR1 GRO 95577 contains the greatest abundance and variety of these nonstandard shapes, many of which were not observed in any other IOM.

Organic nanoglobules also show a wide range of inherent shear strength and plasticity. Most nanoglobules are slightly deformed compared with a perfect sphere, most likely due to deformation from the compressive stresses imposed by the diamond knife during ultramicrotomy, but deformation may have also occurred from differential confining pressure on the asteroid

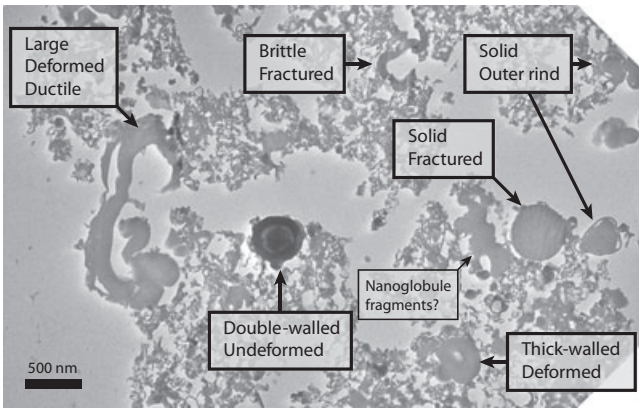

Fig. 3. TEM image of various nanoglobules in GRO 95577 IOM. Many different nanoglobule morphologies are present, including evidence for various levels of plasticity. It should be noted that some of the more exotic morphologies were not observed in IOM from other meteorites in this study and may be unique to GRO 95577.

parent body. In contrast, some nanoglobules are severely deformed, flattened, or broken (Fig. 3). Fractures in nanoglobules are either sharp and angular, indicating a brittle material or characterized by necking and buckling, indicating a ductile material (Fig. 3). Brittle fractures, which were observed in both hollow and solid nanoglobules, are roughly parallel throughout their interiors. These parallel fractures are most likely caused by mechanical vibrations of the diamond knife during ultramicrotomy, also known as "chatter," and would not form in a ductile material. In several IOM residues, most often in IOM from GRO 95577, aspherical, lobate masses are present that may represent an agglomeration of ductile nanoglobule fragments (Fig. 3).

The outer diameters of organic nanoglobules in this study ranged from around 150 nm up to 1150 nm (Fig. 4; Tables 2–8). This size range does not include the oversized

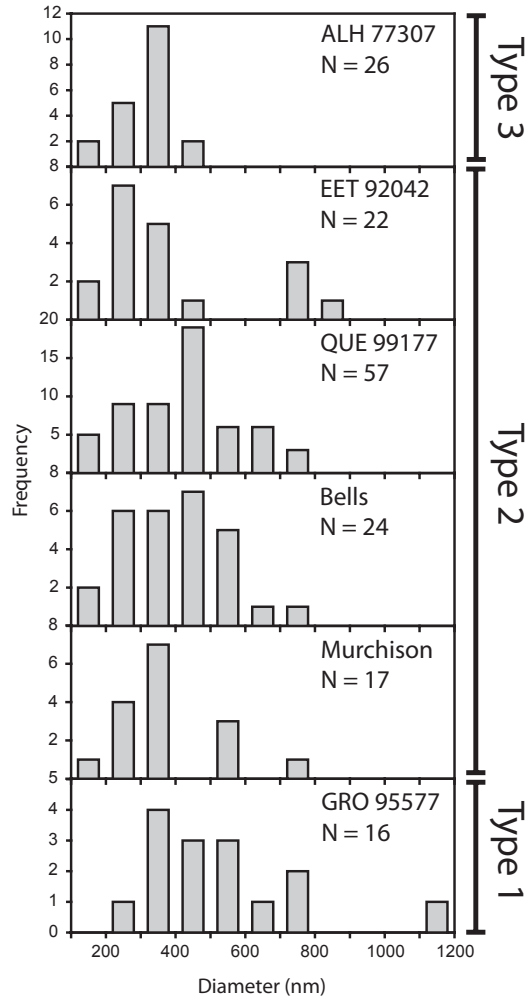

Fig. 4. Size histograms of nanoglobules in six IOM residues. The distributions of nanoglobule diameters are roughly similar for IOM from all type 2 chondrites, but appear to be skewed toward smaller diameters for the less altered type 3 (ALH 77307) and toward larger diameters for the more altered type 1 (GRO 95577).

Table 2. Analyzed nanoglobules in ALH 77307 (with 1σ errors).

Globule	Diameter (nm)	Morphology	Chemistry	$\delta^{13}C$ (‰)	$\delta^{15}N$ (‰)
Bulk IOM			IOM	−8 ± 15	−4 ± 8
Bulk IOM[a]			IOM	−8.29	3.0
2	310	Hollow	IOM-like	n.m.	n.m.
8	420	Hollow	Aromatic	n.m.	n.m.
12	320	Solid	Aromatic	n.m.	n.m.
15h	330	Hollow	IOM-like	n.m.	n.m.
15s	330	Solid	IOM-like	n.m.	n.m.
17	170	Hollow	IOM-like	−64 ± 31	−10 ± 160
18	360	Hollow	Aromatic	−36 ± 30	93 ± 110
20	310	Hollow	Aromatic	n.m.	n.m.
22	320	Hollow	Aromatic	n.m.	n.m.
23	160	Hollow	Aromatic	24 ± 60	7 ± 380

[a]Alexander et al. (2007).
n.m. = not measured.

Table 3. Analyzed nanoglobules in Bells (with 1σ errors).

Globule	Diameter (nm)	Morphology	Chemistry	$\delta^{13}C$ (‰)	$\delta^{15}N$ (‰)	$\delta^{15}N$ (corrected, ‰)
Bulk IOM			IOM	−33 ± 12	151 ± 19	411 ± 21
Bulk IOM[a]			IOM	−34.2	415.3	
2	320	Hollow	n.m.	−332 ± 158	872 ± 94	2365 ± 283
3	720	Hollow	IOM-like	−163 ± 70	89 ± 34	242 ± 93
4	280	Hollow	Aromatic	4 ± 62	603 ± 75	1635 ± 221
5	380	Hollow	n.m.	84 ± 48	284 ± 51	771 ± 145
6	n.m.[b]	Hollow	n.m.	39 ± 36	308 ± 39	837 ± 114
7	480	Hollow	Aromatic	58 ± 51	553 ± 57	1501 ± 173
9	430	Solid	IOM-like	−44 ± 67	169 ± 40	459 ± 111
10	650	Hollow	Aromatic	n.m.	n.m.	
11	400	Hollow	IOM-like	n.m.	n.m.	
13	n.m.[c]	Compound	IOM-like	−52 ± 71	206 ± 39	559 ± 109
14	n.m.[c]	Compound	IOM-like	−100 ± 73	195 ± 38	529 ± 106
16	520	Hollow	IOM-like	3 ± 69	413 ± 35	1120 ± 112
17	530	Hollow	n.m.	−30 ± 103	173 ± 54	470 ± 148
18	570	Hollow	IOM-like	65 ± 95	271 ± 45	734 ± 128
19	410	Hollow	IOM-like	−58 ± 87	549 ± 75	1490 ± 218
22	500	Hollow	IOM-like	61 ± 77	421 ± 88	1142 ± 247
23	330	Hollow	IOM-like	−213 ± 106	17 ± 59	47 ± 160
25	410	Hollow	n.m.	−40 ± 59	500 ± 87	1356 ± 246
26	220	Hollow	n.m.	32 ± 74	493 ± 88	1338 ± 248
27	160	Hollow	n.m.	−9 ± 97	442 ± 54	1199 ± 160
28	590	Hollow	n.m.	−45 ± 89	726 ± 46	1968 ± 162
29	200	Solid	n.m.	−8 ± 121	603 ± 55	1634 ± 171
30	230	Solid	n.m.	−117 ± 136	652 ± 126	1767 ± 355
31	300	Hollow	n.m.	21 ± 103	426 ± 41	1154 ± 127
32	400	Solid	n.m.	112 ± 107	421 ± 54	1143 ± 158
33	290	Hollow	n.m.	−180 ± 86	450 ± 55	1219 ± 162
34	180	Hollow	n.m.	−157 ± 128	561 ± 78	1522 ± 226

[a]Alexander et al. (2007).
[b]This nanoglobule was too deformed to measure an accurate diameter.
[c]Diameters for compound and vermiform nanoglobules were not measured.
n.m. = not measured.

Table 4. Analyzed nanoglobules in EET 92042 (with 1σ errors).

Globule	Diameter (nm)	Morphology	Chemistry	$\delta^{13}C$ (‰)	$\delta^{15}N$ (‰)	$\delta^{15}N$ (corrected, ‰)
Bulk IOM			IOM	−23 ± 10	65 ± 14	175 ± 13
Bulk IOM[a]			IOM	−22.19	184.1	
1	240	Hollow	Aromatic	−2 ± 18	63 ± 39	170 ± 107
4	220	Solid	IOM-like	−9 ± 42	189 ± 92	513 ± 250
6h	260	Hollow	Aromatic	11 ± 34	704 ± 98	1910 ± 284
6s	440	Solid	IOM-like	26 ± 26	26 ± 46	70 ± 125
7	330	Hollow	n.m.	−13 ± 28	40 ± 46	108 ± 124
8	310	Solid	IOM-like	n.m.	n.m.	
10	380	Hollow	Aromatic	−25 ± 33	189 ± 33	514 ± 94
12	810	Hollow	Aromatic	−20 ± 13	300 ± 19	814 ± 67
21	230	Hollow	IOM-like	18 ± 40	207 ± 66	562 ± 182
23	170	Hollow	n.m.	−37 ± 24	533 ± 46	1447 ± 98

[a]Alexander et al. (2007).
n.m. = not measured.

globules with apparent diameters of several μm, which are deformed, flattened, and broken such that an accurate measurement cannot be made. These oversized globules are likely composed of multiple thin-walled nanoglobules, similar to those reported from the Tagish Lake meteorite (Garvie et al. 2008). The largest nanoglobules were

Table 5. Analyzed nanoglobules in GRO 95577 (with 1σ errors).

Globule	Diameter (nm)	Morphology	Chemistry	$\delta^{13}C$ (‰)	$\delta^{15}N$ (‰)	$\delta^{15}N$ (corrected, ‰)
Bulk IOM			IOM	−27 ± 9	91 ± 14	246 ± 15
Bulk IOM[a]			IOM	−26.58	233.2	
1	750	Hollow	IOM-like	38 ± 43	126 ± 26	341 ± 74
2	670	Hollow	IOM-like	−70 ± 74	101 ± 33	275 ± 91
3	700	Hollow	IOM-like	−22 ± 44	184 ± 32	499 ± 90
4	1140	Hollow	IOM-like	−81 ± 38	289 ± 27	785 ± 83
10	510	Solid	IOM-like	58 ± 90	263 ± 64	713 ± 178
11	430	Hollow	Aromatic	47 ± 76	209 ± 73	567 ± 200
12	n.m.[b]	Hollow	IOM-like	−16 ± 39	128 ± 28	346 ± 79
13	320	Hollow	IOM-like	25 ± 69	125 ± 42	339 ± 116
14	380	Hollow	IOM-like	24 ± 65	216 ± 44	586 ± 123
16	350	Hollow	IOM-like	n.m.	n.m.	
17	310	Hollow	n.m.	−77 ± 190	543 ± 131	1472 ± 364
18	250	Hollow	n.m.	−119 ± 256	889 ± 148	2410 ± 421
19	320	Hollow	n.m.	−224 ± 101	602 ± 69	1633 ± 205

[a]Alexander et al. (2007).
[b]This nanoglobule was too deformed to measure an accurate diameter.
n.m. = not measured.

Table 6. Analyzed nanoglobules in Murchison (with 1σ errors).

Globule	Diameter (nm)	Morphology	Chemistry	$\delta^{15}N$ (‰)
Bulk IOM			IOM	−2 ± 1
Bulk IOM[a]			IOM	−1.0
1a	510	Hollow	IOM-like	n.m.
1b	370	Hollow	IOM-like	n.m.
1c	500	Hollow	IOM-like	n.m.
1d	350	Hollow	Aromatic	n.m.
2a1	700	Solid	IOM-like	12 ± 26
2a2	360	Solid	IOM-like	35 ± 44
2b1	210	Hollow	Aromatic	n.m.
2b2	n.m.[b]	Vermiform	IOM-like	n.m.
2b3	380	Hollow	IOM-like	n.m.
2d1	350	Hollow	IOM-like	262 ± 38
2d2	530	Hollow	Aromatic	439 ± 34
2e1	300	Solid	IOM-like	7 ± 35
2e2	350	Solid	IOM-like	17 ± 24
2e3	230	Solid	IOM-like	n.m.
2e4	200	Hollow	IOM-like	n.m.
2e5	160	Solid	IOM-like	n.m.

[a]Alexander et al. (2007)
[b]Diameters for compound and vermiform nanoglobules were not measured.
n.m. = not measured.

observed in IOM from GRO 95577, while IOM from ALH 77307 did not contain any nanoglobules with diameters greater than 500 nm (Fig. 4). As mentioned above, nanoglobules were identified in this study for their suitability for later STXM and SIMS analysis, and thus the observed size distributions are not necessarily representative of the actual nanoglobule size distributions in the various meteorites.

Organic Functional Group Chemistry

XANES analyses of IOM from aqueously altered meteorites (petrologic types 1 and 2) share several spectral characteristics (Cody et al. 2008), including photo-absorption peaks at 285.1, 286.5, and 288.5 eV (Fig. 5). Each of these peaks arises from X-ray-induced excitation of core shell (1*s*) electrons to localized 2*p* π* orbitals of C atoms in distinct bonding environments. For example, the peak at 285.1 eV is generated by C=C double bonds in aromatic moieties (Stöhr 1992). The two peaks at 286.5 and 288.5 eV are commonly assigned to the presence of carbonyl (C=O) bonding in the form of bridging ketones attached to aromatic C, and to bridging or nonbridging carboxyl functional groups, respectively (Urquhart and Ade 2002). In addition, independent analysis of IOM from types 1 and 2 carbonaceous chondrites by nuclear magnetic resonance spectroscopy (Gardinier et al. 2000; Cody et al. 2002, 2011; Cody and Alexander 2005) and infrared spectroscopy (Kebukawa et al. 2010) confirm the presence of both abundant ketone and carboxyl functionality in these samples. Alternatively, the photoabsorption peak around 286.5 eV could be due to the presence of nitrile (C≡N) or some aromatic imine (C=N) bonding (Apen et al. 1993), which have been observed in minor quantities in IOM residues (e.g., Remusat et al. 2005). However, the elemental N abundance in IOM (Alexander et al. 2007) is too low, relative to C, for this spectral feature to be primarily due to N-bearing functionalities.

Table 7. Analyzed nanoglobules in Orgueil (with 1σ errors).

Globule	Diameter (nm)	Morphology	Chemistry	$\delta^{13}C$ (‰)	$\delta^{15}N$ (‰)
Bulk IOM			IOM	−22 ± 1	31 ± 1
Bulk IOM[a]			IOM	−17.05	30.7
1a	150	Hollow	IOM-like	−43 ± 14	20 ± 20
1b	380	Hollow	n.m.	−18 ± 18	154 ± 23
2a	n.m.[b]	Hollow	IOM-like	n.m.	n.m.
2b	380	Hollow	IOM-like	n.m.	n.m.
3a	280	Hollow	IOM-like	−6 ± 53	204 ± 35
3b1	210	Hollow	n.m.	−104 ± 110	−98 ± 112
3b2	250	Hollow	n.m.	85 ± 120	89 ± 93

[a]Alexander et al. (2007).
[b]This nanoglobule was too deformed to measure an accurate diameter.
n.m. = not measured.

Table 8. Analyzed nanoglobules in QUE 99177 (with 1σ errors).

Globule	Diameter (nm)	Morphology	Chemistry	$\delta^{13}C$ (‰)	$\delta^{15}N$ (‰)	$\delta^{15}N$ (corrected, ‰)
Bulk IOM			IOM	−22 ± 7	108 ± 29	187 ± 51
Bulk IOM[a]			IOM	−20.83	187.4	
1	540	Solid	IOM-like	n.m.	n.m.	
2	640	Solid	IOM-like	n.m.	n.m.	
28	180	Hollow	IOM-like	n.m.	n.m.	
29	180	Hollow	Aromatic	16 ± 27	833 ± 159	1445 ± 265
30	430	Solid	IOM-like	−19 ± 18	77 ± 75	134 ± 33
34	270	Hollow	Aromatic	n.m.	n.m.	
36	230	Hollow	IOM-like	−22 ± 23	100 ± 75	174 ± 134
38	350	Solid	IOM-like	−17 ± 21	−2 ± 92	−4 ± 160
39	120	Hollow	IOM-like	n.m.	n.m.	
55	530	Hollow	IOM-like	n.m.	n.m.	
56	530	Hollow	IOM-like	n.m.	n.m.	
57	410	Hollow	Aromatic	n.m.	n.m.	
58	420	Hollow	Aromatic	n.m.	n.m.	
59	230	Hollow	Aromatic	n.m.	n.m.	
67	350	Solid	IOM-like	n.m.	n.m.	
68	310	Hollow	IOM-like	n.m.	n.m.	

[a]Alexander et al. (2007).
n.m. = not measured.

The XANES spectrum of the single type 3.0 chondrite examined in this study, ALH 77307, differs from the other IOM spectra in the absence of the ketone peak at 286.5 eV and a decreased intensity of the carboxyl peak at 288.5 eV (Fig. 5). In addition, an increased intensity of the aromatic peak at 285.1 eV and a steepening of the leading edge of the ionization potential above 290 eV (representing the onset of extended fine structure scattering features) suggest that polyaromatic moieties are larger and more abundant in ALH 77307 IOM. However, these large polyaromatic moieties are not ordered into quasiparallel graphitic domains, as indicated by the lack of a distinct excitonic peak at 291.6 eV (Cody et al. 2008), which is characteristic of graphene, graphite, and semigraphite (Brühwiler et al. 1995; Wessely et al. 2005).

The majority of the organic nanoglobules analyzed in this study exhibit XANES spectra that are similar to their host IOM—specifically, they contain spectral features for aromatic C bonding, aromatic ketones, and carboxyl functional groups (Fig. 5). However, the relative intensities and peak shapes of these spectral features are distinct from those found in bulk IOM XANES spectra. In particular, the aromatic ketone and carboxyl peaks (centered at 286.5 and 288.5 eV, respectively) in the nanoglobule spectra have a higher intensity and a narrower peak shape than the corresponding spectral features from IOM spectra. When the pre-edge XANES data are modeled with a series of Gaussian peaks, the derived peak parameters (e.g., peak height and width) for the nanoglobules cluster together, with slightly larger peak heights and

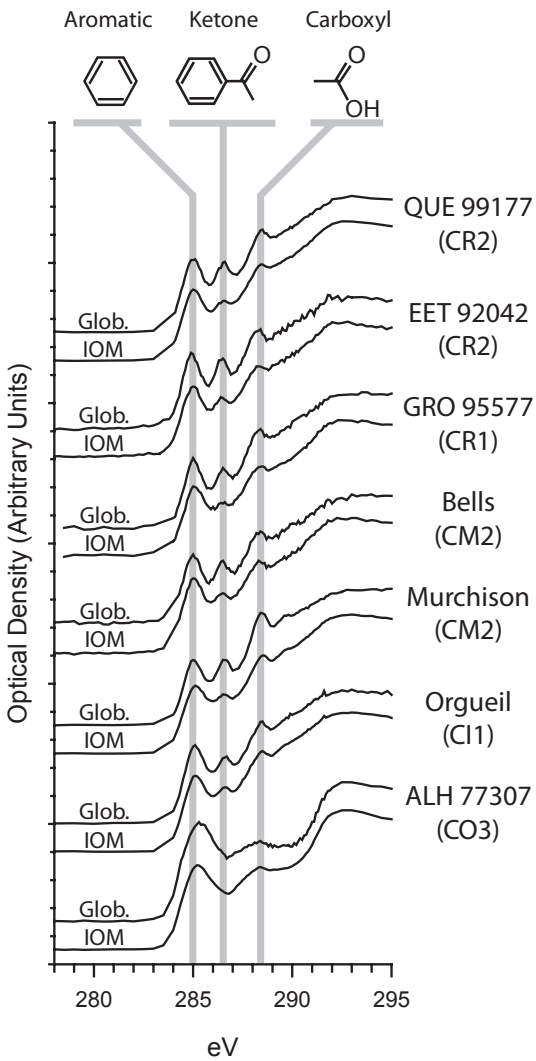

Fig. 5. Average XANES spectra of bulk meteorite IOM and associated organic nanoglobules. Nanoglobules with distinct, highly aromatic functionality have been excluded from the nanoglobule average spectra. To adjust for differences between the two synchrotron facilities (ALS and CLS), spectra were normalized such that the difference in optical density between 280 and 320 eV is equal.

narrower widths for the carbonyl spectral features compared with those of the IOM (Fig. 6). These differences are also visually distinct in averaged XANES spectra of nanoglobules and IOM from the individual meteorites (Fig. 5), and are most pronounced in the CR chondrites and Murchison. The single exception to this trend is the organic nanoglobules in ALH 77307, which are essentially identical to the bulk IOM.

Each of the IOM samples, with the exception of Orgueil, contains one or more nanoglobules with organic functional chemistry distinct from the other nanoglobules and IOM (Tables 2–8). XANES spectra of this separate class of nanoglobules exhibit a much larger and broader aromatic peak centered at a slightly higher X-ray energy (285.2 eV), indicating a higher abundance of aromatic C=C bonding in a wide variety of molecular configurations (Fig. 7). In addition, there is no distinct aromatic ketone absorption at 286.5 eV, nor any distinct intensity at 288.5 eV indicative of carboxyl functionality, and a significant steepening and subsequent flattening of the photo-ionization edge above 290 eV. The combination of these spectral features indicates an overabundance of large aromatic domains at the onset of graphitization, although the lack of a distinct σ* exciton feature indicates that significant aromatization or graphitization has not ensued (De Gregorio et al. 2011). However, the signal quality of the XANES spectra may hide an incipient exciton feature. Due to their distinct spectral features, results from Gaussian peak fitting performed on XANES data from these highly aromatic nanoglobules did not cluster with those from IOM or the majority of the nanoglobules with an IOM-like functionality (Fig. 6), and the final identification of highly aromatic nanoglobules in this study was made based on this semiquantitative basis. The criteria for identifying highly aromatic nanoglobules in ALH 77307 were slightly different, since IOM from this chondrite already contains abundant aromatic material. For ALH 77307 IOM and IOM-like nanoglobules, the XANES peak intensities of the Gaussian fits to the aromatic (285.1 eV) and carboxyl (288.5 eV) features are roughly equivalent. However, the aromatic peak in XANES spectra of the highly aromatic nanoglobules consistently shows a 30–50% increase in intensity relative to the carboxyl peak.

The abundance of highly aromatic nanoglobules relative to nanoglobules with an IOM-like functional chemistry is shown in Fig. 8. Although the low overall population of nanoglobules measured with STXM leads to large error bars (based on Poisson counting statistics), there is an apparent trend of a decreasing relative fraction of aromatic nanoglobules with increasing aqueous alteration.

Isotopic Compositions

The C and N isotopic ratios for the analyzed nanoglobules are provided in Tables 2–8. For bulk samples, reported errors represent one standard error of the mean based on several measurements. Nanoglobule errors are based on counting statistics, reproducibility of standards, and, where relevant, uncertainty in the N contamination correction factor. Most samples showed $\delta^{13}C$ values within errors of solar system values. Two hollow globules in Bells and one in GRO 95529 were observed to have isotopically light C, with $\delta^{13}C$ in the range of −300 to −200‰, but only at the approximately

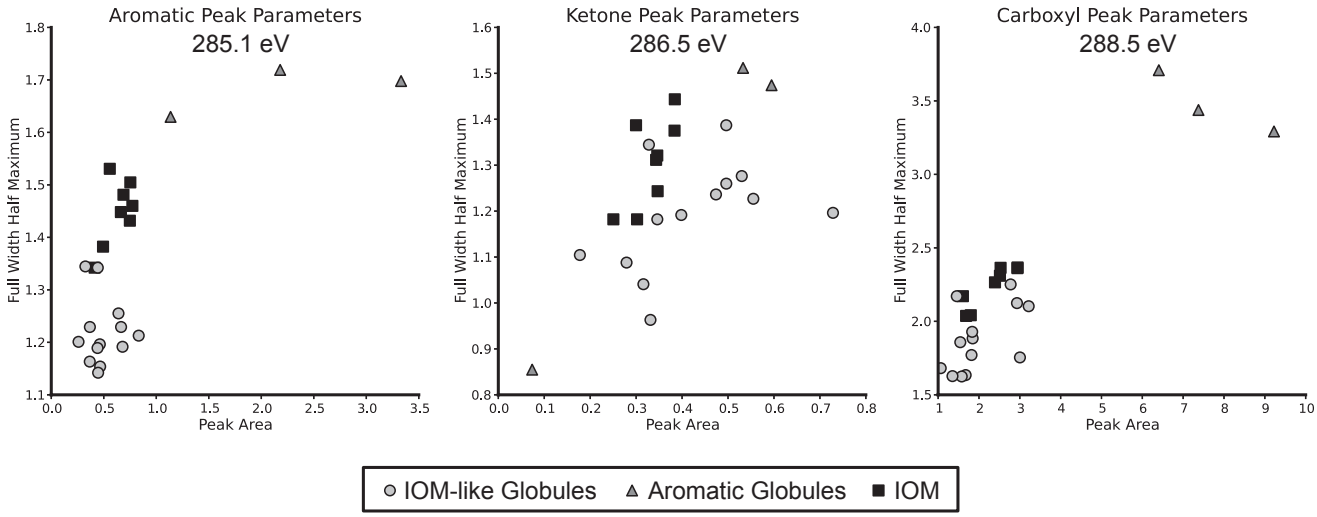

Fig. 6. XANES peak parameters for nanoglobules and IOM from Murchison, derived from Gaussian fits to the three major X-ray absorption features. Peak parameters for nanoglobule spectra tend to cluster separately from those for IOM spectra.

2σ level, so the statistical significance of these results is not strong. This result is consistent with previous work indicating that C isotopic anomalies are rare in meteoritic IOM (Floss et al. 2004; Busemann et al. 2006; Zega et al. 2010), except for in the most primitive CR3 chondrites (Floss and Stadermann 2009).

Isotopic "hotspots" with enriched $^{15}N/^{14}N$ ratios, relative to the bulk IOM, were observed in each of the residues analyzed in this study. In many cases, these hotspots could be correlated to the locations of organic nanoglobules identified previously in TEM images (Fig. 9; Tables 2–8). However, roughly two thirds of the ^{15}N-rich hotspots in each residue were associated with nonglobular IOM (Fig. 10A). The highest ^{15}N enrichments (corrected for terrestrial contamination) in nanoglobules were observed in IOM from GRO 95577 ($\delta^{15}N = 2468 \pm 411‰$) and Bells ($\delta^{15}N = 2422 \pm 261‰$), whereas the largest ^{15}N enrichments within any of the residues we examined were observed in nonglobular hotspots ($\delta^{15}N = 2504 \pm 363‰$ in GRO 95577 and $\delta^{15}N = 4849 \pm 204‰$ in Bells). The range of isotopic hotspot compositions is consistent with previous studies (Busemann et al. 2006; Floss and Stadermann 2009), indicating that the ^{15}N correction applied to the NanoSIMS measurements has not introduced significant errors. In addition, many nanoglobules in each residue were not enriched in ^{15}N relative to the surrounding IOM. The relative proportion of nanoglobules with elevated $^{15}N/^{14}N$ varied between the different chondrites, but generally increased from 30 – 40% in IOM from Murchison and Orgueil to over 80% in IOM from GRO 95577 (Fig. 10B). No ^{15}N-rich nanoglobules were found in IOM from ALH 77307, although another survey of N isotopic hotspots in this meteorite has discovered probable ^{15}N-rich nanoglobules (Bose et al. 2011). It is clear from this dataset that not all organic nanoglobules are isotopically anomalous, nor can isotopically anomalous nanoglobules account for all (or even most) of the ^{15}N hotspots in IOM from primitive meteorites.

Figure 11 compares the N isotopic compositions of nanoglobules, IOM, and nonglobular hotspots. In each of the five IOM residues analyzed by NanoSIMS, the largest ^{15}N enrichments in nanoglobules are of a comparable magnitude to the nonglobular isotopic hotspots (Fig. 11A). Similarly, significant ^{15}N enrichments were observed within both hollow and solid nanoglobules. Subtle differences are observed between nanoglobules with distinct organic functionality (Fig. 11B). Although highly aromatic nanoglobules are in most cases less abundant than IOM-like nanoglobules, they tend to contain higher $^{15}N/^{14}N$ ratios than IOM-like nanoglobules (Fig. 11B).

DISCUSSION

It has been proposed that nanoglobules formed in a variety of environments, such as the interstellar medium and/or the outer solar nebula (Nakamura-Messenger et al. 2006; De Gregorio et al. 2010; Matrajt et al. 2012), in asteroidal parent bodies (Cody et al. 2011), or even as condensed particles around other stars (Garvie and Buseck 2004; Saito and Kimura 2009). One potential way to distinguish between these possibilities is to look for systematic variations of nanoglobule properties amongst and between carbonaceous chondrite groups. For

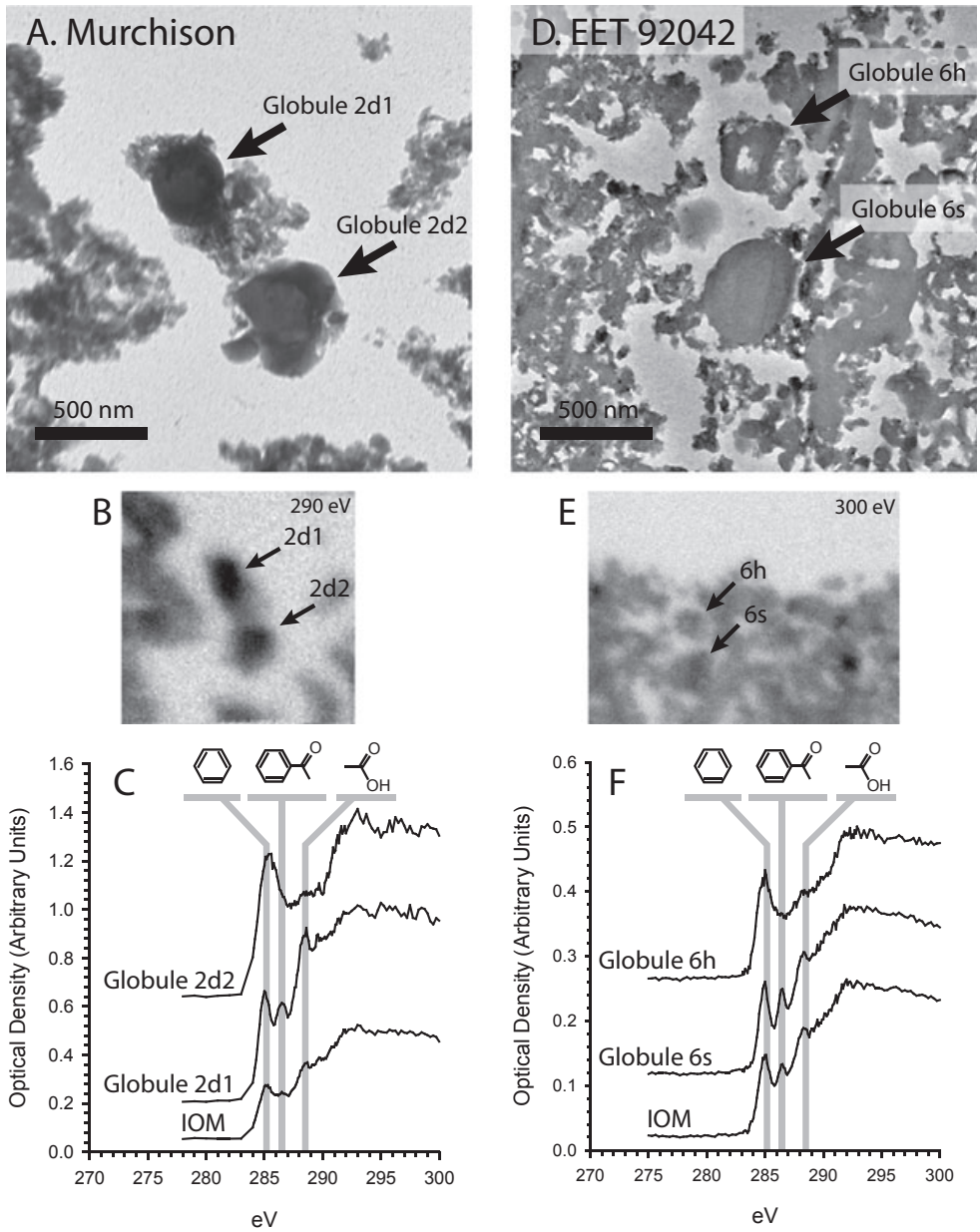

Fig. 7. Comparison of highly aromatic and IOM-like nanoglobules. A) Bright-field TEM image; B) STXM image; and C) XANES spectra of two hollow nanoglobules in Murchison IOM (previously reported by De Gregorio et al. 2010). There are no clear morphological differences between the aromatic and IOM-like nanoglobules. D) Bright-field TEM image, E) STXM image, and F) XANES spectra of a hollow and a solid nanoglobule in EET 92042 IOM.

instance, if nanoglobules are interstellar in origin, the types, sizes, and relative abundances of globules should be similar in all chondrites. If nanoglobules formed in the solar nebula, their properties may vary with the time and position of the chondrite parent bodies, but should be relatively uniform within a chondrite group. If nanoglobules formed primarily within parent bodies, their properties may vary depending on the organic content and water/organic ratio at the time of accretion, and will ultimately be strongly correlated with the chemistry and isotopic composition of the host IOM. Of course, the primary features of nanoglobules that formed prior to accretion may also have been modified by aqueous alteration and thermal metamorphism during their residence on the parent asteroid. Here, we attempt to ascertain whether there exist any systematic variations in nanoglobule properties, and, if so, whether they can be used to constrain their origin.

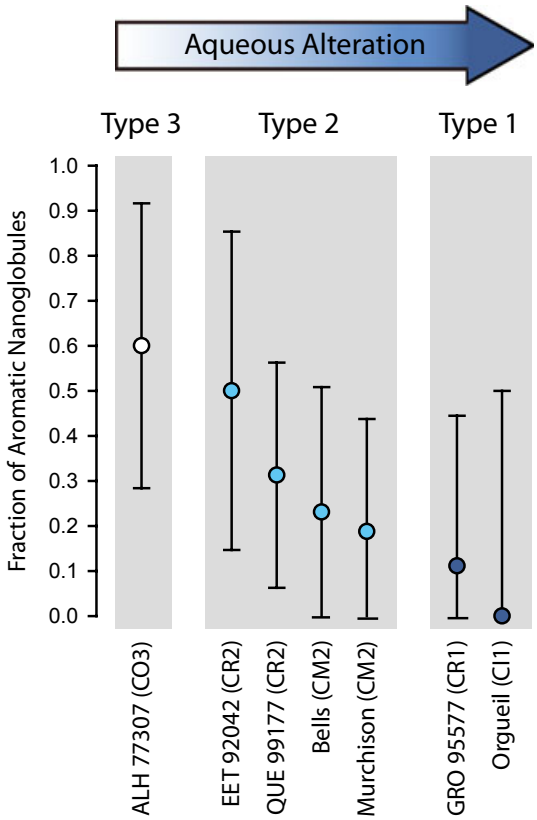

Fig. 8. Relative abundances of nanoglobules with a highly aromatic functional chemistry, grouped by alteration type. Error bars are calculated from Poisson sampling statistics.

Classification of Nanoglobules

Most of the organic nanoglobules can be grouped into one of three major categories, based primarily on their functional chemistry and isotopic compositions, each of which may have a distinct formation and alteration history. For each meteorite we studied, there is a main population of nanoglobules that shares a similar, although slightly more oxygenated, functional chemistry and range of ^{15}N isotopic compositions as the host IOM. A second subset of nanoglobules was also present in all meteorites except Orgueil, which are clearly distinguished from the IOM and IOM-like nanoglobules by their highly aromatic functional chemistry. These aromatic nanoglobules have as high as or, in many cases, higher ^{15}N enrichments than the IOM and IOM-like nanoglobules. The functional group chemistry of these features may be unique, as no analogous sub-μm, nonglobular, highly aromatic, or graphitic domains of IOM were observed. It is interesting to note that, with the exception of a single solid nanoglobule, all of the globules with a highly aromatic functional chemistry have a typical hollow morphology. The presence of a faint ring in the center of this single solid aromatic globule suggests that it may in fact be an ultramicrotome slice near the edge of a hollow nanoglobule, barely intersecting the hollow interior (Fig. 12). If correct, all of the highly aromatic nanoglobules identified in this study are hollow. The third category of nanoglobules comprises those with an IOM-like functional chemistry, but also with an N isotope composition clearly enriched in ^{15}N compared with the corresponding IOM composition. Despite the clear differences between IOM-like and aromatic functional chemistry in the XANES data, all of these nanoglobule groupings share the same range of sizes. Although we suggest that all of the aromatic nanoglobules are hollow, at present both functional group chemistries were observed in both solid and hollow nanoglobules. Thus, making a distinction between the three groupings is impossible based solely on observations of globular morphology.

Parent Body Alteration and Nanoglobule Morphology and Chemistry

Organic nanoglobules are prevalent in each of the studied meteorite IOM residues, which span a range of petrologic type from the relatively unaltered aqueously, but slightly metamorphosed, CO 3.0 ALH 77307 to the highly aqueously altered chondrites, CI1 Orgueil and CR1 GRO 95577. In general, these data suggest that the size distribution of nanoglobules changes with parent-body aqueous alteration (Fig. 4), with the smallest nanoglobule diameters observed in the IOM from the least altered chondrite (ALH 77307), and the largest nanoglobule diameters observed in the IOM from one of the most altered chondrites (GRO 95577). All of the IOM from type 2 meteorites appears to have a similar distribution of nanoglobule sizes, even though CR chondrite IOM is generally held to be more primitive than that in CM chondrites (Cody and Alexander 2005; Busemann et al. 2006; Alexander et al. 2007). However, as described previously, the necessity to identify large, isolated nanoglobules for STXM and NanoSIMS analysis introduced a size bias against smaller globules. Thus, the size distributions of nanoglobules in each of the IOM residues (Fig. 4) may not accurately reproduce the full distribution of the total population of nanoglobules in each sample. Additional studies are necessary to determine whether nanoglobule population statistics significantly differ between parent bodies or vary as a function of aqueous alteration (e.g., Changela et al. 2012).

Nanoglobule functional chemistry also appears to be affected by aqueous alteration on the parent body. The ratio of highly aromatic nanoglobules to IOM-like nanoglobules appears to decrease with increasing

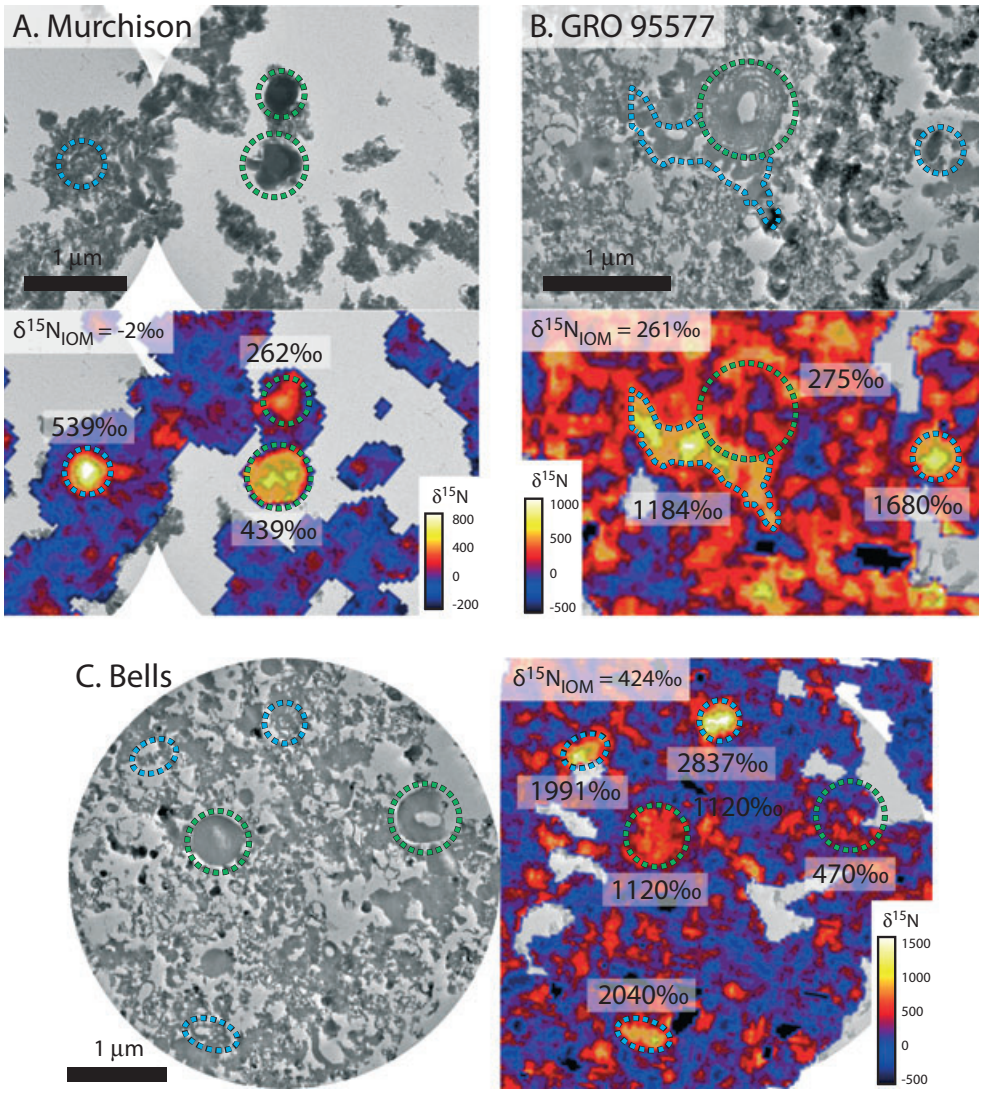

Fig. 9. Correlated bright-field TEM images and $^{15}N/^{14}N$ isotopic maps measured by NanoSIMS. Organic nanoglobules are identified by green circles, while nonglobular, isotopically anomalous regions are identified by blue circles. Nitrogen isotopic compositions ($\delta^{15}N$ values) are listed adjacent to each region. A) Region of Murchison IOM containing ^{15}N-enriched nanoglobules 2d1 (upper globule) and 2d2 (lower globule). B) Region of GRO 95577 IOM containing "nanoporous" nanoglobule 2. C) Region of Bells IOM containing nanoglobules 16 (left) and 17 (right).

parent-body alteration (Fig. 8), although again it is not clear whether this difference is statistically significant given the small sample size. In fact, a counter trend was observed in the Tagish Lake chondrite, where proportionally higher abundances of aromatic nanoglobules were observed in lithologies containing greater evidence of aqueous alteration (Herd et al. 2011), although the sample populations were limited in that study as well. The more primitive chondrites within each petrologic type also appear to contain relatively more aromatic nanoglobules, with the CR chondrites containing a proportionally higher aromatic fraction than the CM chondrites (Fig. 8). This trend can be attributed to one of two mechanisms: (1) highly aromatic nanoglobules were preferentially destroyed by aqueous alteration, or (2) additional IOM-like nanoglobules (with relatively lower aromaticity) were created during periods of aqueous alteration on the parent body. In the first scenario, the overall abundance of nanoglobules should decrease with increased hydrothermal processing, while the opposite trend would be observed in the second scenario. However, given the generally stable nature of aromatic molecules, relative to other organic functional groups, the former scenario is unlikely.

The higher abundance of aromatic material in ALH 77307 relative to the other chondrites in this study (Fig. 8) may be due to greater thermal metamorphism

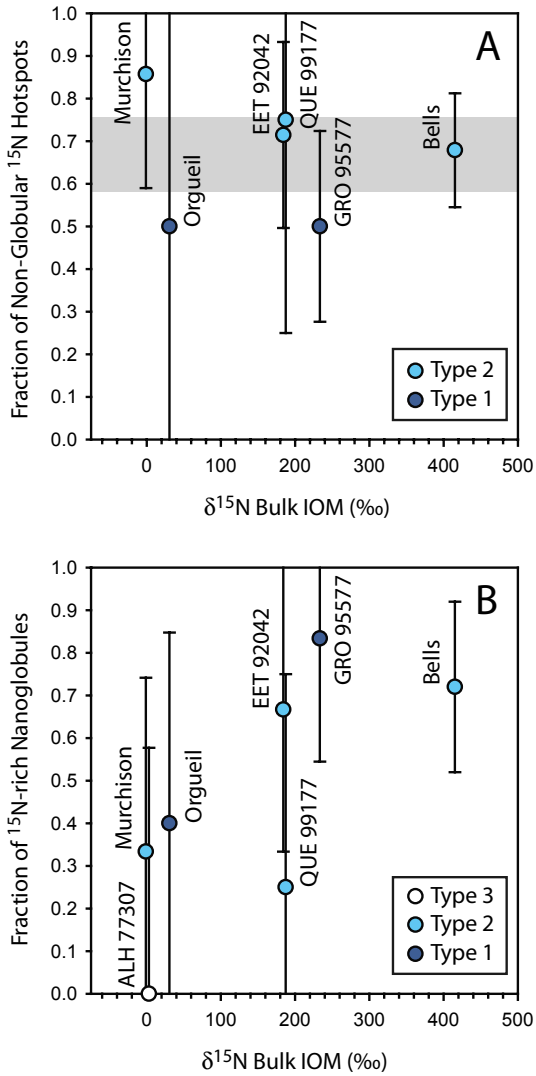

Fig. 10. A) Fraction of ^{15}N-rich hotspots that cannot be attributed to organic nanoglobules. Data for ALH 77307 are absent because no nonglobular hotspots were observed in this IOM residue. The gray band represents the average value across all samples. B) Fraction of nanoglobules that contain significant ^{15}N enrichments over bulk IOM. Error bars are calculated from Poisson sampling statistics for each dataset. Errors for the measured δ^{15}N values are smaller than the size of the data points.

on the ALH 77307 parent body. Studies of IOM from other CO3 chondrites, such as Kainsaz (CO3.6), have shown significant reduction in oxidized functional groups relative to IOM from types 1 and 2 carbonaceous chondrites (Cody et al. 2008; Remusat et al. 2008). In these meteorites, thermal metamorphism has visibly contributed to aromatization and carbonization of the IOM (Kebukawa et al. 2011; Le Guillou et al. 2012), with a concurrent reduction in noncarbon heteroatoms. However, petrographic studies of ALH 77307 have concluded that, although the meteorite has experienced heating to higher temperatures than type 1 and 2 chondrites, it has not experienced temperatures greater than 200 °C (Huss et al. 2006), and therefore significant graphitization or aromatization of IOM is not expected to have occurred. Direct analyses of IOM from ALH77307 by Raman and XANES spectroscopy have estimated similar temperatures of 220 °C (Busemann et al. 2007) and 203 ± 41 °C (Cody et al. 2008), respectively.

Nitrogen Isotopic Characteristics of Nanoglobules

Unlike their morphology and organic functionality, the isotopic composition of nanoglobules is strongly correlated with the chondrite group rather than petrologic type. Previous studies have suggested that organic nanoglobules are preferentially composed of D- and ^{15}N-enriched material and are the source of many of the D- and ^{15}N-rich carbonaceous hotspots observed in primitive astromaterials (Nakamura-Messenger et al. 2006; Messenger et al. 2008; Busemann et al. 2009). However, this study is the first correlated high-resolution survey of the isotopic compositions for a large number of nanoglobules across several meteorite samples, and, in general, we found that the majority of ^{15}N hotspots (roughly two thirds) are localized in nonglobular IOM (Fig. 10A). A similar result was found during a correlated TEM/NanoSIMS study of the primitive CR chondrite MET 00426 (Floss et al. 2011). Organic nanoglobules therefore are not the predominant carrier of the most ^{15}N-rich material. In addition, not all nanoglobules contain anomalous N isotopic signatures. While most nanoglobules (roughly 75%) in the more primitive chondrites, EET 92042, GRO 95577, and Bells, contained some ^{15}N enrichment above the bulk IOM isotopic compositions, less than approximately 40% of the nanoglobules in Murchison and Orgueil were found to be enriched in ^{15}N (Fig. 10B).

As shown in Fig. 11B, most of the nanoglobules with aromatic functional group chemistry were enriched in ^{15}N well above bulk IOM enrichments. Considering the IOM samples in which these highly aromatic nanoglobules were observed, the nanoglobule with the largest ^{15}N enrichment also contained aromatic functional group chemistry in all but one sample. Highly aromatic organic matter with a ^{15}N-rich isotopic composition has also been observed in samples from comet Wild 2, including a coating on a sulfide grain (Matrajt et al. 2008) and a nanoglobule (De Gregorio et al. 2010). The organic chemical functionality of a few other ^{15}N-rich carbonaceous features with globule-like morphologies in Wild 2 samples are either not aromatic or undetermined (Matrajt et al. 2008, 2010). In

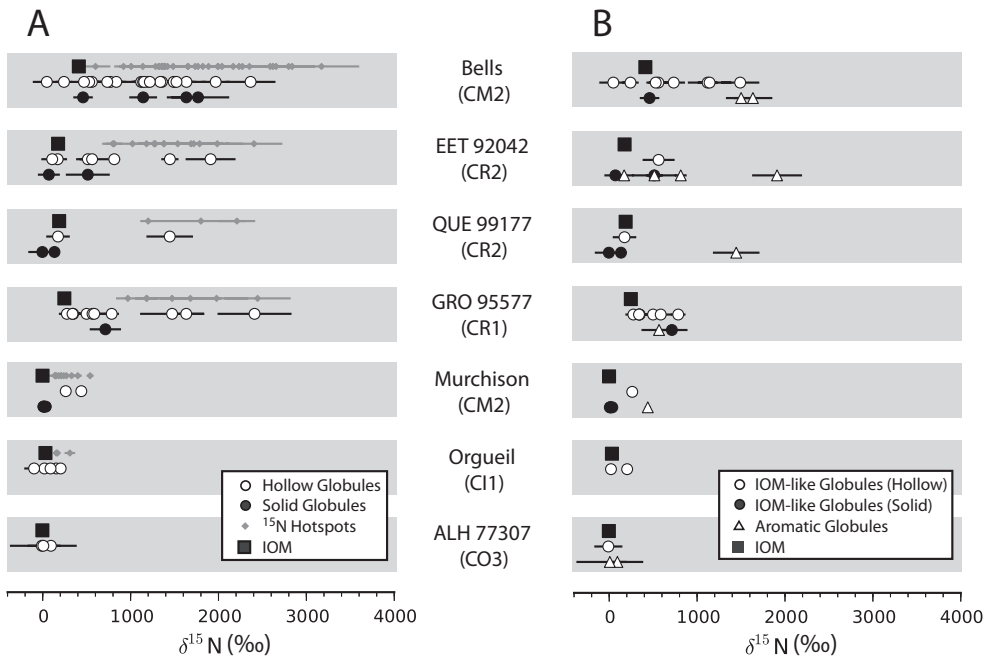

Fig. 11. N isotopic composition of organic nanoglobules relative to bulk IOM. A) Comparison of hollow and solid nanoglobules with other, nonglobular ^{15}N hotspots. B) Comparison of hollow and solid nanoglobules for which the organic functional chemistry is also known. Meteorite samples are listed in terms of decreasing "primitiveness" as defined by a combination of bulk D and ^{15}N isotopic excess (Alexander et al. 2007) and alteration type. For Bells and the CR chondrites, the plotted values are the isotope ratios corrected for terrestrial contamination, as described in the text. True values for these samples may be lower, but the relative trends between different meteorites and nanoglobules would remain the same.

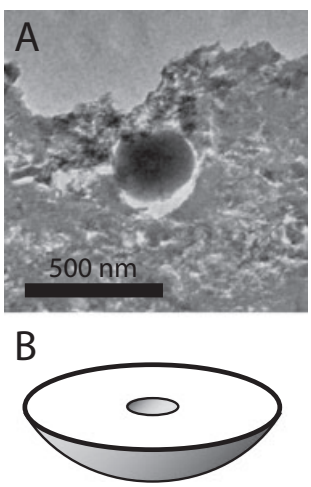

Fig. 12. A) Globule 12 in the IOM residue from ALH 77307 is the only example of a solid nanoglobule with a highly aromatic functional chemistry. However, the presence of a small faint ring in the center and the radial brightness profile indicating thinner material near the edges of the nanoglobule suggests that this feature may actually be an ultramicrotome slice from the edge of a hollow nanoglobule. B) A graphical representation of such an ultramicrotome slice taken from the edge of a hollow globule.

combination, these studies suggest that highly aromatic organic grains, most likely in the form of nanoglobules, were a ubiquitous, although minor, component of early nebular material. This material is distinct from presolar graphite grains, which contain an extremely large range of C isotopic compositions (Hoppe et al. 1995; Bernatowicz et al. 1996; Croat et al. 2005) that are not observed in ^{15}N-rich aromatic organic matter and nanoglobules.

Mechanisms of Nitrogen Isotopic Fractionation in Nanoglobule Precursor Material

The similar distributions of both nanoglobules and nonglobular isotopic hotspots indicate that the extreme ^{15}N enrichments in each of them were derived from similar processes. The two major mechanisms often invoked to explain such enrichments are ion-molecule chemistry in cold molecular cloud environments (Terzieva and Herbst 2000; Charnley and Rodgers 2002) and N_2 self-shielding in the early solar nebula (Lyons et al. 2009). As current self-shielding models can only produce ^{15}N enrichments up to $\delta^{15}N = 800‰$, the process cannot explain the isotopic compositions of ^{15}N-rich nanoglobules, which often exceed $\delta^{15}N = 1000‰$ (Tables 2–8; Fig. 11). However, as self-shielding models are further developed, the maximum fractionation achievable by this method may increase (cf. Muskatel et al. 2011). Similarly, ion-molecule

reactions occurring in typical molecular cloud environments can only produce modest ^{15}N enrichments (Terzieva and Herbst 2000). However, in cold cloud cores where the temperature is low enough to freeze out CO (approximately 10 K), extreme ^{15}N enrichments in excess of $\delta^{15}N = 2000‰$ may be preserved in ammonia and nitrile monolayers at different evolutionary stages on icy grains (Rodgers and Charnley 2008). According to this model, the outermost ammonia layers will have peak $\delta^{15}N$ values between 3000‰ and 10,000‰ (Rodgers and Charnley 2008). Since this fractionation would have occurred prior to the formation of the protosun, the observed N isotopic compositions of the most ^{15}N-rich hotspots (including nanoglobules) could represent presolar interstellar chemistry. Although significant nitrile functionality was not observed, it is likely that a small amount of ^{15}N-enriched interstellar nitrile groups are present in ^{15}N-enriched nanoglobules. However, the tendency for highly aromatic nanoglobules to contain ^{15}N isotopic anomalies suggests that much of this material has been converted into aromatic moieties.

Aléon (2010) argued, on the basis of H and N isotopic trends in astromaterials, that organic matter in carbonaceous chondrites, IDPs, and comets is largely a mixture of material enriched in D and ^{15}N from low-temperature ion-molecule reactions occurring in the outer protoplanetary disk and extremely ^{15}N-enriched material fractionated by an as-yet-unknown mechanism occurring in warmer regions of the protosolar disk. The latter component is represented by ^{15}N hotspots in IOM without large accompanying D enrichments and by ^{15}N-rich clasts from the Isheyevo CH/CB chondrite (Briani et al. 2009; Bonal et al. 2010), and it was argued to have formed and been added late in nebular history (Aléon 2010). An interstellar origin for the most ^{15}N-rich material is considered to be unlikely by Aléon (2010) because gas-phase HCN and NH_3 in dense molecular clouds and protostars are not observed to be enriched in ^{15}N (Güsten and Ungerechts 1985; Dahmen et al. 1995; Gerin et al. 2009; Lis et al. 2010). However, recent observations of CN and HNC in molecular clouds have shown ^{15}N enrichments up to around 1200‰ (Adande and Ziurys 2012) and recent observations of nitriles in cold dense prestellar cores have shown significant fractionation for both N and D (Hirota et al. 2001; Milam and Charnley 2012). The lack of ^{15}N enrichment in NH_3 may reflect the evolutionary state of the prestellar cores (Rodgers and Charnley 2008). It is also possible that the average isotopic composition of gas-phase N-bearing interstellar molecules does not reflect the isotopic composition of grain-adsorbed, N-bearing molecules, which are mostly invisible to astronomers unless they are one of the predominant phases. Aléon (2010) also argued that an interstellar ^{15}N source is unlikely because at the low temperatures required for extreme ^{15}N enrichments via ion-molecule reactions (Rodgers and Charnley 2008), H isotopes in the gas would be also expected to be highly fractionated (Herbst 2003), generating correlated D excesses. Ion-molecule isotopic fractionation proceeds via a complex network of reactions, which are currently still poorly constrained. Recent calculations suggest that the spin-state energy between different spin configurations of H_2 can account for anticorrelated D and ^{15}N enrichments (Wirström et al. 2012). Moreover, D/H is more rapidly equilibrated during aqueous alteration than is $^{15}N/^{14}N$ (Herd et al. 2011; Robert et al. 2011; Kebukawa and Cody 2012), particularly if the ^{15}N is preserved in stable aromatic heterocycles. Thus, ion-molecule reactions in cold molecular cloud cores or the outermost reaches of the protosolar disk are still the most likely process for generating the extreme ^{15}N-rich isotopic compositions observed in IOM hotspots, including ^{15}N-rich organic nanoglobules.

The large range of N isotopic ratios observed in nanoglobules and at sub-μm scales in IOM indicates that such interstellar and/or protostellar signatures are either not uniformly incorporated or not uniformly preserved in chondrites. As observed in previous surveys from several carbonaceous meteorites, certain chondrite groups (specifically, the CR chondrites and the anomalous CM Bells) contain IOM with higher D/H and $^{15}N/^{14}N$ ratios, and a greater abundance of D- and/or ^{15}N-rich isotopic hotspots (Robert and Epstein 1982; Yang and Epstein 1983; Busemann et al. 2006; Alexander et al. 2007). Alexander et al. (2007) argued that, based on chemical and isotopic trends of IOM across different meteorite groups, that the different groups most likely accreted a common D- and ^{15}N-enriched organic precursor that was subsequently modified by parent-body processing. The sub-μm isotopic heterogeneity observed in IOM may reflect heterogeneity in the organic precursor material originally accreted by the meteorite parent bodies or variable processing due to transport in the solar nebula (e.g., Remusat et al. 2010), overprinted by subsequent parent-body processing. Studies of anhydrous porous IDPs, which are believed to be more primitive than even the least altered carbonaceous chondrites, contain little evidence for parent-body processing (Messenger 2000; Bradley 2003). Yet organic matter even in these primitive anhydrous IDPs exhibits extreme H and N isotopic heterogeneity on the sub-μm scale (Aléon et al. 2003; Floss et al. 2004, 2006; Messenger et al. 2008; Busemann et al. 2009; Matrajt et al. 2012), as well as a range of morphologies (including nanoglobules; Messenger et al. 2008; Floss et al. 2011; Matrajt et al.

2012) and similar C-XANES spectra to those observed in meteoritic IOM (Flynn et al. 2003; Busemann et al. 2009). On meteorite parent bodies, this primitive isotopic distribution is strongly affected by parent-body processing (Alexander et al. 1998; Sephton et al. 2003; Bonal et al. 2010), as observed directly in a comparative study of several subsamples of the Tagish Lake meteorite (Zega et al. 2010; Herd et al. 2011). This aqueous processing likely overprinted the general chemistry and composition of organic nanoglobules as well. Nevertheless, the most ^{15}N-enriched materials (including ^{15}N-rich nanoglobules), in combination with D-enriched objects, clearly contain the best-preserved record of the various isotopic enrichment processes, and their isotopic compositions will allow us to put constraints on these processes.

Preaccretionary Formation of Nanoglobule Structures

Previous studies have suggested several mechanisms for the formation of the typical hollow nanoglobule morphology, mainly focusing on the irradiation of organic matter on the surface of icy grains (Nakamura-Messenger et al. 2006; De Gregorio et al. 2010; Matrajt et al. 2012). Experimental irradiation of N-rich organic/ice mixtures by protons (Moore et al. 1983) or UV photons (Dworkin et al. 2001; Bernstein et al. 2002; Dartois et al. 2005; Nuevo et al. 2011) has established that there is a synthesis of more complex organics from mixtures of simple, interstellar-like precursor molecules. Continued irradiation may eventually generate sub-μm grains of macromolecular organic matter, although the observed chemistry of these processed organics has not matched the functional group profiles of nanoglobules or bulk IOM. Nakamura-Messenger et al. (2006) hypothesized that the outer few hundred nm could be processed to the point that a single coherent organic layer was formed, after which the removal of the interior ice and volatiles would result in a hollow, spherical, nanoglobule. This model is convenient as it generates nanoglobules in the same environment where ^{15}N enrichments are expected to be formed. Aside from the fact that it has not yet been demonstrated that such a process can generate materials with the physical or chemical characteristics of nanoglobules, criticisms of this model include: (1) icy grains in molecular clouds are not necessarily spherical, but rather are likely to have fractal structures (Fogel and Leung 1998); (2) icy grains include fine-grained silicate and other mineral dust, which are not observed within nanoglobules; (3) it requires an unreasonable balance between the generation of coherent, homogenous, macromolecular organic matter and highly permeable organic matter; and (4) surface processing of a thick organic rind will most likely create a layered structure as material is added to the grain surface and through the attenuation of UV photons with depth. We note that such a mechanism has also not been shown to produce solid globules.

A high-energy mechanism for nanoglobule formation, suggested by Garvie and Buseck (2004) and tested experimentally by Saito and Kimura (2009), is based on the injection of simple PAH molecules into a He plasma. Hollow particles composed of amorphous C with outer diameters of less than 150 nm were created, suggesting that nanoglobule-like objects could form around evolved stars. Although the laboratory-produced objects have a smaller size range than naturally occurring nanoglobules, this could simply reflect the scale of the experimental apparatus. While the chemical functionality of these objects was not characterized, they likely retain some of the aromatic functionality of their precursor PAHs, since similar plasma experiments result in larger PAHs generated via a polymerization mechanism (Shih et al. 2005). However, the primary stellar sources of carbonaceous dust, C-rich asymptotic giant branch stars, are depleted in D and ^{15}N due to prior H burning (Busso et al. 1999; Meyer and Zinner 2006), unlike the observed isotopically anomalous nanoglobules. Excesses in ^{15}N are observed in carbonaceous presolar grains from supernovae and novae (Hoppe et al. 1995; Amari et al. 2001; Lin et al. 2010), but these stars are also highly depleted in D, and no D-depleted nanoglobules have ever been reported. Subsequent D enrichment of the entire mass of a nanoglobule in molecular cloud or outer nebular environments is not kinetically favorable and difficult to envision. Furthermore, presolar graphite grains in Murchison contain ^{12}C/^{13}C ratios that vary by over three orders of magnitude (Hoppe et al. 1995; Bernatowicz et al. 1996; Croat et al. 2005), while the δ^{13}C values observed in nanoglobules cluster around the solar value. Thus, nanoglobule formation in circumstellar environments around dust-producing stars cannot explain the observed occurrence of D-enriched organic nanoglobules with a solar ^{12}C/^{13}C.

It is also possible that nanoglobule structures can form in nebular environments from existing IOM precursor material. The observation that nanoglobule morphology and N isotopic composition are not always coupled could be explained by a two-step process. First, IOM precursor material is delivered to the contracting presolar molecular cloud from a variety of source regions, some of which is isotopically enriched in ^{15}N. These organics would most likely have been introduced as discrete particles, which then would have been heterogeneously mixed to form the overall reservoir of

nebular organic matter. A nebular nanoglobule-forming process could then operate on this reservoir, generating a diverse nanoglobule population, including highly aromatic and IOM-like functional chemistry, with various levels of ^{15}N enrichment depending on which organic particles from the nebular reservoir are incorporated. The remainder of the nebular reservoir would then be accreted into planetesimals and other parent bodies as nonglobular IOM and would contain copious nonglobular isotopic hotspots. Unfortunately, there is currently no known or hypothesized mechanism to form nanoglobule morphologies within the presolar nebula. Such a process could be similar to the plasma condensation model proposed by Saito and Kimura (2009), operating in energetic environments near the protosun, or it could potentially be related to high-temperature, high-pressure, chondrule-forming events. Simulations of the UV irradiation environment of icy grains within the nebula indicate that synthesis of significant amounts of complex organic molecules will take place (Ciesla and Sandford 2012), although it is not clear that this process could also generate globular objects.

Postaccretionary Formation and Modification of Nanoglobules

The presence of larger nanoglobules (Fig. 4) and the widest variety of globule morphologies in IOM from one of the more altered meteorites (GRO 95577; Fig. 3) suggests that some organic nanoglobules have been generated during aqueous alteration on the parent bodies. This must be a complex process, since similar nanoglobule morphologies were not observed in Orgueil, which also experienced intense alteration on its parent body (Tomeoka and Buseck 1988). A postaccretionary origin for nanoglobules has been suggested previously by Cody et al. (2011). In such a model, secondary organic nanoglobules could be generated initially from soluble organic matter, including original accreted material or breakdown products from altered IOM. Whether the precursor material was accreted or formed in the parent body, a polymerization mechanism is necessary to form the nanoglobule morphology. At present, the most promising of these mechanisms is the formose reaction involving formaldehyde (Cody et al. 2011). Through formaldehyde chemistry, Cody et al. (2011) generated an IOM-like material containing spherical nanoglobules with organic functionality nearly identical to that of IDPs and primitive IOM. Some amphiphilic (lipid-like) molecules generated by UV irradiation of methanol- and ammonia-containing interstellar ice mixtures can also self-assemble into vesicles when dispersed into aqueous fluids (Dworkin et al. 2001). However, the chemistry of these irradiated residues are distinct from that of IOM and IOM-like nanoglobules, and the morphology of these vesicles, being constructed of a thin lipid bilayer with a relatively large enclosed void, is not consistent with nanoglobule morphologies. In addition, amphiphilic vesicles do not persist after the fluids are removed, but rather they disassemble to form organic films. Finally, this soluble amphiphilic material would not be expected to be present in IOM isolates like those we have studied. In asteroid parent bodies, postaccretionary nanoglobules would be expected to have IOM-like functional groups and contain similar isotopic signatures as bulk IOM, unless isotopic exchange took place during their formation. Thus, a postaccretionary formation of organic nanoglobules would not produce aromatic nanoglobules, and the fraction of aromatic nanoglobules should be anticorrelated with the amount of aqueous alteration, of which we observe only a weak trend in our data (Fig. 8).

Postaccretionary globular structures derived from chemical reactions occurring on parent bodies (including formose chemistry) would tend to reflect the bulk ^{15}N enrichment of IOM, and therefore the fraction of nanoglobules with extreme ^{15}N enrichments should decrease as aqueous processing continues. Our data (Fig. 10B) do not show such a correlation. There are notably fewer ^{15}N-rich nanoglobules in IOM from Murchison and Orgueil (Fig. 10B), both of which have experienced significant parent-body processing, and the $^{15}N/^{14}N$ ratio of these enriched nanoglobules is severely decreased compared with those in the other chondrites in this study (Fig. 11A). However, no significant distinction is present between the relative abundance and ^{15}N enrichments of nanoglobules in the highly altered GRO 95577 (CR1) and less altered EET 92042 (CR2). In addition, no ^{15}N-rich nanoglobules were observed in the least aqueously altered chondrite, ALH 77307 (CO3), although the absence of these globules could be due to low sampling statistics, since several ^{15}N-rich nanoglobules have recently been reported in this meteorite (Bose et al. 2011). It must be noted that, due to the relatively small sample set of nanoglobules that were analyzed with NanoSIMS, these data may not be statistically significant. Yet even within this limited dataset, a weak correlation is present between the fraction of ^{15}N-rich nanoglobules and the bulk ^{15}N enrichment of IOM (Fig. 10B), suggesting that the overall isotopic compositions of nanoglobules are more reflective of the original accreted IOM precursor material rather than later chemical reactions that occurred on the parent bodies. This view is further supported by the observation of extreme ^{15}N

enrichments in IOM-like nanoglobules (i.e., the nanoglobules most likely to have been formed on the parent body; Fig. 11B). Although a strong case can be made for a preaccretionary origin of aromatic nanoglobules and ^{15}N-rich nanoglobules with IOM-like functional group chemistry, it is still unclear whether the remainder of the IOM-like nanoglobules formed in preaccretionary environments or within the asteroid parent body.

Extant primary nanoglobules also appear to be modified during aqueous processing by accumulation of additional organic matter, as indicated by the presence of thin, organic rinds around some hollow and solid nanoglobules (Fig. 3). The thin-walled, hollow nanoglobules that are common in GRO 95577 IOM may result from this modification process, after the original interior nanoglobules, around which the rims formed, are removed. The interior nanoglobules may be preferentially "plucked out" during ultramicrotomy of the IOM residue, leaving the secondary organic rind behind. Accumulation of organic matter in rims, coatings, and other modification of extant nanoglobules may explain the observed trend of the general increase in nanoglobule diameters with the degree of parent-body processing (Fig. 4). This mechanism also raises the possibility of the existence of highly aromatic nanoglobules with IOM-like organic rinds. Unfortunately, the spatial resolution of the STXM instrument is not adequate to distinguish the functional groups present in the thin organic rinds from those in the bulk nanoglobule. Future TEM-based electron energy-loss measurements using monochromated sources could address this possibility.

CONCLUSION

The 184 organic nanoglobules observed in this study contain a variety of morphologies, organic functional group chemistries, and N isotopic compositions. In addition to the "classic" hollow spherical morphology, nanoglobules can also take the form of solid spheres and other unusual morphologies. While most nanoglobules are composed of carbonaceous matter with similar organic functionality to the surrounding bulk carbonaceous matter in the meteorite, a small but statistically significant subset of them are composed of a distinct, highly aromatic carbonaceous matter. Similarly, most nanoglobules lack ^{15}N isotopic enrichments that are indicative of molecular cloud chemistry, while a subset of nanoglobules contains ^{15}N enrichments up to the levels frequently observed in nonglobular ^{15}N isotopic hotspots. However, correlated TEM and SIMS analyses show that the overwhelming majority of hotspots are attributed to nonglobular carbonaceous matter. The lack of a single well-defined class of nanoglobules contrasts with their descriptions in previous research (e.g., Nakamura-Messenger et al. 2006) and makes it unlikely that a single mechanism was responsible for their formation. The observed correlations between nanoglobule diameter, functional group chemistry, and meteorite alteration type appear to be independent of chondrite class, and therefore suggest a general influence of parent-body aqueous alteration on these particular nanoglobule properties rather than preaccretionary differences between individual parent bodies. On the other hand, the proportion of nanoglobules that are enriched in ^{15}N is most strongly correlated with chondrite class and bulk ^{15}N enrichment, rather than with alteration type, indicating the accretion of nanoglobules with presolar heritages. These contrasting trends suggest that the morphological properties of nanoglobules may have been shaped in both preaccretionary and asteroidal environments and may likely be decoupled from the formation of the carbonaceous matter that composes them.

Although it has been hypothesized that extreme ^{15}N enrichments could be generated in nebular environments (Aléon et al. 2003), it is most likely that the most ^{15}N-rich nanoglobules, including both hollow and solid morphologies, as well as both highly aromatic and IOM-like organic chemistry, were formed outside the solar nebula, or at least in the cold outer regions of the nebula where such ^{15}N enrichments are theorized to take place. The highly aromatic nanoglobules, which tend to carry the greatest ^{15}N enrichments, may represent discrete carbonaceous grains predating the formation of the solar system and later accreted onto planetesimals. Thus, although not likely formed in circumstellar environments, these ^{15}N-rich aromatic nanoglobules may be considered a new category of interstellar presolar grains.

Acknowledgments—We sincerely thank Drs. L. Remusat, G. Matrajt, N. Johnson, and associate editor C. Floss for their constructive reviews. This work was supported by the Office of Naval Research, NASA Cosmochemistry and Origins of Solar Systems Programs, and the NASA Astrobiology Institute. This research was conducted while the primary author held a National Research Council Research Associateship at the U.S. Naval Research Laboratory. Use of the Advanced Light Source was supported by the U.S. Department of Energy. Use of the Canadian Light Source was supported by the Natural Sciences and Engineering Research Council of Canada, the National Research Council Canada, the Canadian Institutes of Health Research, the Province of

Saskatchewan, Western Economic Diversification Canada, and the University of Saskatchewan.

Editorial Handling—Dr. Christine Floss

REFERENCES

Adande G. R. and Ziurys L. M. 2012. Millimeter-wave observations of CN and HNC and their ^{15}N isotopologues: A new evaluation of the ^{14}N/^{15}N ratio across the galaxy. *The Astrophysical Journal* 744:194 (15 pp.).

Aléon J. 2010. Multiple origins of nitrogen isotopic anomalies in meteorites and comets. *The Astrophysical Journal* 722:1342–1351.

Aléon J., Robert F., Chaussidon M., and Marty B. 2003. Nitrogen isotopic composition of macromolecular organic matter in interplanetary dust particles. *Geochimica et Cosmochimica Acta* 67:3773–3783.

Alexander C. M. O'D., Russell S. S., Arden J. W., Ash R. D., Grady M. M., and Pillinger C. T. 1998. The origin of chondritic macromolecular organic matter: A carbon and nitrogen isotope study. *Meteoritics & Planetary Science* 33:603–622.

Alexander C. M. O'D., Fogel M., Yabuta H., and Cody G. D. 2007. The origin and evolution of chondrites recorded in the elemental and isotopic compositions of their macromolecular organic matter. *Geochimica et Cosmochimica Acta* 71:4380–4403.

Alpern B. and Benkheiri Y. 1973. Distribution de la matière organique dans la météorite d'Orgueil par microscopie en fluorescence. *Earth and Planetary Science Letters* 19:422–428.

Amari S., Gao X., Nittler L. R., Zinner E., Jose J., Hernanz M., and Lewis R. S. 2001. Presolar grains from novae. *The Astrophysical Journal* 551:1065–1072.

Aoki T. and Akai J. 2008. Carbon materials in Antarctic and nonAntarctic carbonaceous chondrites: High-resolution transmission electron microscopy. *Journal of Mineralogical and Petrological Sciences* 103:173–182.

Apen E., Hitchcock A. P., and Gland J. L. 1993. Experimental studies of the core excitation of imidazole, 4, 5-dicyanoimidazole, and *s*-triazine. *Journal of Physical Chemistry* 97:6859–6866.

Bassim N. D., De Gregorio B. T., Kilcoyone A. L. D., Scott K., Chou T., Wirick S., Cody G., and Stroud R. M. 2012. Minimizing damage during FIB sample preparation of soft materials. *Journal of Microscopy* 245:288–301.

Bernatowicz T. J., Cowsik R., Gibbons P. C., Lodders K., Fegley B., Amari S., and Lewis R. S. 1996. Constraints on stellar grain formation from presolar graphite in the Murchison meteorite. *The Astrophysical Journal* 472: 760–782.

Bernstein M. P., Dworkin J. P., Sandford S. A., Cooper G. W., and Allamandola L. J. 2002. Racemic amino acids from the ultraviolet photolysis of interstellar ice analogues. *Nature* 416:401–403.

Bonal L., Huss G. R., Krot A. N., Nagashima K., Ishii H. A., and Bradley J. P. 2010. Highly ^{15}N-enriched chondritic clasts in the CB/CH-like meteorite Isheyevo. *Geochimica et Cosmochimica Acta* 74:6590–6609.

Bose M., Floss C., and Stadermann F. 2011. Carbonaceous N-anomalous grains in the CO3.0 meteorite ALHA77307 (abstract #1444). 42nd Lunar and Planetary Science Conference. CD-ROM.

Bradley J. P. 2003. Interplanetary dust particles. In *Meteorites, comets, and planets*, edited by Davis A. M. Oxford: Elsevier-Pergamon. pp. 689–711.

Briani G., Gounelle M., Marrocchi Y., Mostefaoui S., Leroux H., Quirico E., and Meibom A. 2009. Pristine extraterrestrial material with unprecedented nitrogen isotopic variation. *Proceedings of the National Academy of Sciences* 106:10522–10527.

Brownlee D. E., Tsou P., Aléon J., Alexander C. M. O'D., Araki T., Bajt S., Baratta G. A., Bastien R., Bland P., Bleuet P., Borg J., Bradley J. P., Brearley A., Brenker F., Brennan S., Bridges J. C., Browning N. D., Brucato J. R., Bullock E., Burchell M. J., Busemann H., Butterworth A., Chaussidon M., Cheuvront A., Chi M., Cintala M. J., Clark B. C., Clemett S. J., Cody G., Colangeli L., Cooper G., Cordier P., Daghlian C., Dai Z., d'Hendecourt L., Djouadi Z., Dominguez G., Duxbury T., Dworkin J. P., Ebel D. S., Economou T. E., Fakra S., Fairey S. A. J., Fallon S., Ferrini G., Ferroir T., Fleckenstein H., Floss C., Flynn G., Franchi I. A., Fries M., Gainsforth Z., Gallien J.-P., Genge M., Gilles M. K., Gillet P., Gilmour J., Glavin D. P., Gounelle M., Grady M. M., Graham G. A., Grant P. G., Green S. F., Grossemy F., Grossman L., Grossman J. N., Guan Y., Hagiya K., Harvey R., Heck P., Herzog G. F., Hoppe P., Hörz F. P., Huth J., Hutcheon I. D., Ignatyev K., Ishii H. A., Ito M., Jacob D., Jacobsen C., Jacobsen S., Jones S., Joswiak D., Jurewicz A., Kearsley A. T., Keller L. P., Khodja H., Kilcoyne A. L. D., Kissel J., Krot A., Langenhorst F., Lanzirotti A., Le L., Leshin L. A., Leitner J., Lemelle L., Leroux H., Liu M.-C., Luening K., Lyon I., MacPherson G., Marcus M. A., Marhas K., Marty B., Matrajt G., McKeegan K., Meibom A., Mennella V., Messenger K., Messenger S., Mikouchi T., Mostefaoui S., Nakamura T., Nakano T., Newville M., Nittler L. R., Ohnishi I., Ohsumi K., Okudaira K., Papanastassiou D. A., Palma R., Palumbo M. E., Pepin R. O., Perkins D., Perronnet M., Pianetta P., Rao W., Rietmeijer F. J. M., Robert F., Rost D., Rotundi A., Ryan R., Sandford S. A., Schwandt C. S., See T. H., Schlutter D., Sheffield-Parker J., Simionovici A., Simon S., Sitnitsky I., Snead C. J., Spencer M. K., Stadermann F. J., Steele A., Stephan T., Stroud R., Susini J., Sutton S. R., Suzuki Y., Taheri M., Taylor S., Teslich N., Tomeoka K., Tomioka N., Toppani A., Trigo-Rodriguez J. M., Troadec D., Tsuchiyama A., Tuzzolino A. J., Tyliszczak T., Uesugi K., Velbel M., Vellenga J., Vicenzi E., Vincze L., Warren J., Weber I., Weisberg M., Westphal A. J., Wirick S., Wooden D., Wopenka B., Wozniakiewicz P., Wright I., Yabuta H., Yano H., Young E. D., Zare R. N., Zega T., Ziegler K., Zimmerman L., Zinner E., and Zolensky M. 2006. Comet 81P/Wild 2 under a microscope. *Science* 314:1711–1716.

Brühwiler P. A., Maxwell A. J., Puglia C., Nilsson A., Anderson S., and Mårtensson N. 1995. π^* and σ^* excitons in C 1*s* absorption of graphite. *Physical Review Letters* 74:614–617.

Busemann H., Young A. F., Alexander C. M. O'D., Hoppe P., Mukhopadhyay S., and Nittler L. R. 2006. Interstellar chemistry recorded in organic matter from primitive meteorites. *Science* 312:727–730.

Busemann H., Alexander C. M. O'D., and Nittler L. R. 2007. Characterization of insoluble organic matter in primitive

meteorites by microRaman spectroscopy. *Meteoritics & Planetary Science* 42:1387–1416.

Busemann H., Nguyen A. N., Cody G. D., Hoppe P., Kilcoyne A. L. D., Stroud R. M., Zega T. J., and Nittler L. R. 2009. Ultra-primitive interplanetary dust particles from the comet 26P/Grigg-Skjellerup dust stream collection. *Earth and Planetary Science Letters* 288:44–57.

Busso M., Gallino R., and Wasserburg G. J. 1999. Nucleosynthesis in asymptotic giant branch stars: Relevance for galactic enrichment and solar system formation. *Annual Review of Astronomy and Astrophysics* 37:239–309.

Changela H., Stroud R. M., Peeters Z., Nittler L. R., Alexander C. M. O'D., De Gregorio B. T., and Cody G. D. 2012. Morphological study of insoluble organic matter residues from primitive chondrites (abstract #2745). 43rd Lunar and Planetary Science Conference. CD-ROM.

Charnley S. B. and Rodgers S. D. 2002. The end of interstellar chemistry as the origin of nitrogen in comets and meteorites. *The Astrophysical Journal Letters* 569: L133–L137.

Ciesla F. J. and Sandford S. A. 2012. Organic synthesis via irradiation and warming of ice grains in the solar nebula. *Science* 336:452–454.

Claus G. and Nagy B. 1961. A microbiological examination of some carbonaceous chondrites. *Nature* 192:594–596.

Cody G. D. and Alexander C. M. O'D. 2005. NMR studies of chemical structural variation of insoluble organic matter from different carbonaceous chondrite groups. *Geochimica et Cosmochimica Acta* 69:1085–1097.

Cody G. D., Alexander C. M. O'D., and Tera F. 2002. Solid-state (^{1}H and ^{13}C) nuclear magnetic resonance spectroscopy of insoluble organic residue in the Murchison meteorite: A self-consistent quantitative analysis. *Geochimica et Cosmochimica Acta* 66:1851–1865.

Cody G. D., Alexander C. M. O'D., Yabuta H., Kilcoyne A. L. D., Araki T., Ade H., Dera P., Fogel M., Militzer B., and Mysen B. O. 2008. Organic thermometry for chondritic parent bodies. *Earth and Planetary Science Letters* 272:446–455.

Cody G. D., Brandes J., Jacobsen C., and Wirick S. 2009. Soft X-ray induced chemical modification of polysaccharides in vascular plant cell walls. *Journal of Electron Spectroscopy and Related Phenomena* 170:57–64.

Cody G. D., Heying E., Alexander C. M. O'D., Nittler L. R., Kilcoyne A. L. D., Sandford S. A., and Stroud R. M. 2011. Establishing a molecular relationship between chondritic and cometary organic solids. *Proceedings of the National Academy of Sciences* 108:19171–19176.

Croat T. K., Stadermann F. J., and Bernatowicz T. J. 2005. Presolar graphite from AGB stars: Microstructure and *s*-process enrichment. *The Astrophysical Journal* 631:976–987.

Dahmen G., Wilson T. L., and Matteucci F. 1995. The nitrogen isotope abundance in the galaxy: I. The galactic disk gradient. *Astronomy & Astrophysics* 295:194–198.

Dartois E., Muñoz Caro G. M., Deboffle D., Montagnac G., and d'Hendecourt L. 2005. Ultraviolet photoproduction of ISM dust: Laboratory characterization and astrophysical relevance. *Astronomy & Astrophysics* 432:895–908.

De Gregorio B. T., Stroud R. M., Nittler L. R., Alexander C. M. O'D., Kilcoyne A. L. D., and Zega T. J. 2010. Isotopic anomalies in organic nanoglobules from comet 81P/Wild 2: Comparison to Murchison nanoglobules and isotopic anomalies induced in terrestrial organics by electron irradiation. *Geochimica et Cosmochimica Acta* 74: 4454–4470.

De Gregorio B. T., Sharp T. G., Rushdi A. I., and Simoneit B. R. T. 2011. Bugs or gunk? Nanoscale methods for assessing the biogenicity of ancient microfossils and organic matter. In *Earliest life on Earth: Habitats, environments and methods of detection*, edited by Golding S. D. and Glikson M. Dordrecht, the Netherlands: Springer. pp. 239–289.

Dworkin J. P., Deamer D. W., Sandford S. A., and Allamandola L. J. 2001. Self-assembling amphiphilic molecules: Synthesis in simulated interstellar/precometary ices. *Proceedings of the National Academy of Sciences* 98:815–819.

Floss C. and Stadermann F. J. 2009. High abundance of circumstellar and interstellar C-anomalous phases in the primitive CR3 chondrites QUE 99177 and MET 00426. *The Astrophysical Journal* 697:1242–1255.

Floss C., Stadermann F. J., Bradley J., Dai Z. R., Bajt S., and Graham G. 2004. Carbon and nitrogen isotopic anomalies in an anhydrous interplanetary dust particle. *Science* 303:1355–1358.

Floss C., Stadermann F. J., Bradley J. P., Dai Z. R., Bajt S., Graham G., and Lea A. S. 2006. Identification of isotopically primitive interplanetary dust particles: A NanoSIMS isotopic imaging study. *Geochimica et Cosmochimica Acta* 70:2371–2399.

Floss C., Le Guillou C., Stadermann F. J., and Brearley A. J. 2011. Coordinated NanoSIMS and TEM analyses of C- and N-anomalous phases in the CR3 chondrite MET 00426 (abstract #1455). 42nd Lunar and Planetary Science Conference. CD-ROM.

Flynn G. J., Keller L. P., Feser M., Wirick S., and Jacobsen C. 2003. The origin of organic matter in the solar system: Evidence from the interplanetary dust particles. *Geochimica et Cosmochimica Acta* 67:4791–4806.

Fogel M. E. and Leung C. M. 1998. Modeling extinction and infrared emission from fractal dust grains: Fractal dimension as a shape parameter. *The Astrophysical Journal* 501:175–191.

Gardinier A., Derenne S., Robert F., Behar F., Largeau C., and Maquet J. 2000. Solid state CP/MAS ^{13}C NRM of the insoluble organic matter of the Orgueil and Murchison meteorites: Quantitative study. *Earth and Planetary Science Letters* 184:9–21.

Garvie L. A. J. 2006. Extraterrestrial carbon nanospheres. *Carbon* 44:158–160.

Garvie L. A. J. and Buseck P. R. 2004. Nanosized carbon-rich grains in carbonaceous chondrite meteorites. *Earth and Planetary Science Letters* 224:431–439.

Garvie L. A. J., Baumgardner G., and Buseck P. R. 2008. Scanning electron microscopical and cross-sectional analysis of extraterrestrial carbonaceous nanoglobules. *Meteoritics & Planetary Science* 43:899–903.

Gerin M., Marcelino N., Biver N., Roueff E., Coudert L. H., Elkeurti M., Lis D. C., and Bockelée-Morvan D. 2009. Detection of $^{15}NH_2D$ in dense cores: A new tool for measuring the $^{14}N/^{15}N$ ratio in the cold ISM. *Astronomy & Astrophysics* 498:L9–L12.

Güsten R. and Ungerechts H. 1985. Constraints on the sites of nitrogen nucleosynthesis from $^{15}NH_3$-observations. *Astronomy & Astrophysics* 145:241–250.

Herbst E. 2003. Isotopic fractionation by ion-molecule reactions. *Space Science Reviews* 106:293–304.

Herd C. D. K., Blinova A., Simkus D. N., Huang Y., Tarozo R., Alexander C. M. O'D., Gyngard F., Nittler L. R., Cody G. D., Fogel M. L., Kebukawa Y., Kilcoyne A. L. D., Hilts R. W., Slater G. F., Glavin D. P., Dworkin J. P., Callahan M. P., Elsila J. E., De Gregorio B. T., and Stroud R. M. 2011. Origin and evolution of prebiotic organic matter as inferred from the Tagish Lake meteorite. *Science* 332:1304–1307.

Hirota T., Ikeda M., and Yamamoto S. 2001. Observations of DNC and $HN^{13}C$ in dark cloud cores. *The Astrophysical Journal* 547:814–828.

Hoppe P., Amari S., Zinner E., and Lewis R. S. 1995. Isotopic compositions of C, N, O, Mg, and Si, trace element abundances, and morphologies of single circumstellar graphite grains in four density fractions from the Murchison meteorite. *Geochimica et Cosmochimica Acta* 59:4029–4056.

Huss G. R., Rubin A. E., and Grossman J. N. 2006. Thermal metamorphism in chondrites. In *Meteorites and the early solar system II*, edited by Lauretta D. S. and McSween H. Y., Jr. Tucson, Arizona: The University of Arizona Press. pp. 567–586.

Jacobsen C., Wirick S., Flynn G. J., and Zimba C. 2000. Soft X-ray spectroscopy from image sequences with sub-100 nm spatial resolution. *Journal of Microscopy* 197:173–184.

Kaznatcheev K. V., Karunakaran C., Lanke U. D., Urquhart S. G., Obst M., and Hitchcock A. P. 2007. Soft X-ray spectromicroscopy beamline at the CLS: Commissioning results. *Nuclear Instruments and Methods in Physics Research Section A* 582:96–99.

Kebukawa Y. and Cody G. D. 2012. Deuterium-hydrogen exchange kinetics: Implications for early chemical evolution of chondritic insoluble organic matter (abstract #1034). 43rd Lunar and Planetary Science Conference. CD-ROM.

Kebukawa Y., Nakashima S., and Zolensky M. E. 2010. Kinetics of organic matter degradation in the Murchison meteorite for the evaluation of parent-body temperature history. *Meteoritics & Planetary Science* 45:99–113.

Kebukawa Y., Alexander C. M. O'D., and Cody G. D. 2011. Compositional diversity in insoluble organic matter in type 1, 2 and 3 chondrites as detected by infrared spectroscopy. *Geochimica et Cosmochimica Acta* 75: 3530–3541.

Kilcoyne A. L. D., Tyliszczak T., Steele W. F., Fakra S., Hitchcock P., Franck K., Anderson E., Harteneck B., Rightor E. G., Mitchell G. E., Hitchcock A. P., Yang L., Warwick T., and Ade H. 2003. Interferometer-controlled scanning transmission X-ray microscopes at the Advanced Light Source. *Journal of Synchrotron Radiation* 10:125–136.

Le Guillou C., Rouzaud J.-N., Bonal L., Quirico E., Derenne S., and Remusat L. 2012. High resolution TEM of chondritic carbonaceous matter: Metamorphic evolution and heterogeneity. *Meteoritics & Planetary Science* 47:345–362.

Lin Y., Gyngard F., and Zinner E. 2010. Isotopic analysis of supernova SiC and Si_3N_4 grains from the Qingzhen (EH3) chondrite. *The Astrophysical Journal* 709:1157–1173.

Lis D. C., Wootten A., Gerin M., and Roueff E. 2010. Nitrogen isotopic fractionation in interstellar ammonia. *The Astrophysical Journal Letters* 710:L49–L52.

Lyons J. R., Bergin E. A., Ciesla F. J., Davis A. M., Desch S. J., Hashizume K., and Lee J.-E. 2009. Timescales for the evolution of oxygen isotope compositions in the solar nebula. *Geochimica et Cosmochimica Acta* 73: 4998–5017.

Matrajt G., Ito M., Wirick S., Messenger S., Brownlee D. E., Joswiak D., Flynn G., Sandford S., Snead C., and Westphal A. 2008. Carbon investigation of two Stardust particles: A TEM, NanoSIMS, and XANES study. *Meteoritics & Planetary Science* 43:315–334.

Matrajt G., Messenger S., Ito M., Wirick S., Flynn G. J., Joswiak D. J., and Brownlee D. E. 2010. TEM, XANES and NanoSIMS characterization of carbonaceous phases from individual Stardust and IDP particles (abstract #1564). 41st Lunar and Planetary Science Conference. CD-ROM.

Matrajt G., Messenger S., Brownlee D., and Joswiak D. 2012. Diverse forms of primordial organic matter identified in interplanetary dust particles. *Meteoritics & Planetary Science* 47:525–549.

Maurette M. 1998. Carbonaceous micrometeorites and the origin of life. *Origins of Life and Evolution of Biopsheres* 28:385–412.

Messenger S. 2000. Identification of molecular-cloud material in interplanetary dust particles. *Nature* 404:968–971.

Messenger S., Nakamura-Messenger K., and Keller L. P. 2008. ^{15}N-rich organic globules in a cluster IDP and the Bells CM2 chondrite (abstract #2391). 39th Lunar and Planetary Science Conference. CD-ROM.

Meyer B. S. and Zinner E. 2006. Nucleosynthesis. In *Meteorites and the early solar system II*, edited by Lauretta D. S. and McSween H. Y., Jr. Tucson, Arizona: The University of Arizona Press. pp. 69–108.

Milam S. N. and Charnley S. B. 2012. Observations of nitrogen fractionation in prestellar cores: Nitriles tracing interstellar chemistry (abstract #2618). 43rd Lunar and Planetary Science Conference. CD-ROM.

Moore M. H., Donn B., Khanna R., and A'Hearn M. F. 1983. Studies of proton-irradiated cometary-type ice mixtures. *Icarus* 54:388–405.

Muskatel B. H., Remacle F., Thiemens M. H., and Levine R. D. 2011. On the strong and selective isotope effect in the UV excitation of N_2 with implications toward the nebula and Martian atmosphere. *Proceedings of the National Academy of Sciences* 108:6020–6025.

Nakamura K., Zolensky M. E., Tomita S., Nakashima S., and Tomeoka K. 2002. Hollow organic globules in the Tagish Lake meteorite as possible products of primitive organic reactions. *International Journal of Astrobiology* 1:179–189.

Nakamura-Messenger K., Messenger S., Keller L. P., Clemett S. J., and Zolensky M. E. 2006. Organic globules in the Tagish Lake meteorite: Remnants of the protosolar disk. *Science* 314:1439–1442.

Nuevo M., Milam S. N., Sandford S. A., De Gregorio B. T., Cody G. D., and Kilcoyne A. L. D. 2011. XANES analysis of organic residues produced from the UV irradiation of astrophysical ice analogs. *Advances in Space Research* 48:1126–1135.

Peeters Z., Changela H. G., Stroud R. M., Alexander C. M. O'D., and Nittler L. R. 2012. Coordinated analysis on *in situ* organic material in the CR chondrite QUE 99177 (abstract #2612). 43rd Lunar and Planetary Science Conference. CD-ROM.

Remusat L., Derenne S., Robert F., and Knicker H. 2005. New pyrolitic and spectroscopic data on Orgueil and Murchison

insoluble organic matter: A different origin than soluble? *Geochimica et Cosmochimica Acta* 69:3919–3932.

Remusat L., Le Guillou C., Rouzaud J.-N., Binet L., Derenne S., and Robert F. 2008. Molecular study of insoluble organic matter in Kainsaz CO3 carbonaceous chondrite: Comparison with CI and CM IOM. *Meteoritics & Planetary Science* 43:1099–1111.

Remusat L., Guan Y., Wang Y., and Eiler J. M. 2010. Accretion and preservation of D-rich organic particles in carbonaceous chondrites: Evidence for important transport in the early solar system. *The Astrophysical Journal* 713:1048–1058.

Robert F. and Epstein S. 1982. The concentration and isotopic composition of hydrogen, carbon and nitrogen in carbonaceous meteorites. *Geochimica et Cosmochimica Acta* 46:81–95.

Robert F., Derenne S., Thomen A., Anquetil C., and Hassouni K. 2011. Deuterium exchange rate between D_3^+ and organic CH bonds: Implication for D enrichment in meteoritic IOM. *Geochimica et Cosmochimica Acta* 75:7522–7532.

Rodgers S. D. and Charnley S. B. 2008. Nitrogen superfractionation in dense cloud cores. *Monthly Notices of the Royal Astronomical Society Letters* 385:L48–L52.

Rossignol-Strick M. and Barghoorn E. S. 1971. Extra terrestrial abiogenic organization of organic matter: The hollow spheres of the Orgueil meteorite. *Origins of Life and Evolution of Biospheres* 3:89–107.

Saito M. and Kimura Y. 2009. Origin of organic globules in meteorites: Laboratory simulation using aromatic hydrocarbons. *The Astrophysical Journal Letters* 703: L147–L151.

Sephton M. A., Verchovsky A. B., Bland P. A., Gilmour I., Grady M. M., and Wright I. P. 2003. Investigating the variations in carbon and nitrogen isotopes in carbonaceous chondrites. *Geochimica et Cosmochimica Acta* 67:2093–2108.

Shih S.-I., Lin T.-C., and Shih M. 2005. Decomposition of benzene in the RF plasma environment: Part II. Formation of polycyclic aromatic hydrocarbons. *Journal of Hazardous Materials* 117:149–159.

Stöhr J. 1992. *NEXAFS spectroscopy*. Berlin: Springer.

Tasch P. 1963. Identity of organized elements in carbonaceous chondrites. *Science* 142:156–158.

Terzieva R. and Herbst E. 2000. The possibility of nitrogen isotopic fractionation in interstellar clouds. *Monthly Notices of the Royal Astronomical Society* 317:563–568.

Tomeoka K. and Buseck P. R. 1988. Matrix mineralogy of the Orgueil CI carbonaceous chondrite. *Geochimica et Cosmochimica Acta* 52:1627–1640.

Urquhart S. G. and Ade H. 2002. Trends in the carbonyl core (C 1S, O 1S) $\rightarrow \pi^*_{C=O}$ transition in the near-edge X-ray absorption fine structure spectra of organic molecules. *Journal of Physical Chemistry B* 106:8531–8538.

Wessely O., Katsnelson M. I., and Eriksson O. 2005. Ab initio theory of dynamical core-hole screening in graphite from X-ray absorption spectra. *Physical Review Letters* 94:167401 (4 pp.).

Wirick S., Flynn G. J., Keller L. P., Nakamura-Messenger K., Peltzer C., Jacobsen C., Sandford S., and Zolensky M. 2009. Organic matter from comet 81P/Wild 2, IDPs, and carbonaceous meteorites; similarities and differences. *Meteoritics & Planetary Science* 44:1611–1626.

Wirström E. S., Charnley S. B., Cordiner M. A., and Milam S. N. 2012. Isotopic anomalies in primitive solar system matter: Spin-state-dependent fractionation of nitrogen and deuterium in interstellar clouds. *The Astrophysical Journal Letters* 757:L11 (5 pp.).

Yang J. and Epstein S. 1983. Interstellar organic matter in meteorites. *Geochimica et Cosmochimica Acta* 47:2199–2216.

Zega T. J., Alexander C. M. O'D., Busemann H., Nittler L. R., Hoppe P., Stroud R. M., and Young A. F. 2010. Mineral associations and character of isotopically anomalous organic material in the Tagish Lake carbonaceous chondrite. *Geochimica et Cosmochimica Acta* 74:5966–5983.